NACA RM E52J31

RESEARCH MEMORANDUM

EXPERIMENTAL INVESTIGATION OF RADOME ICING AND ICING PROTECTION

By James P. Lewis and Robert J. Blade

Lewis Flight Propulsion Laboratory
Cleveland, Ohio

NATIONAL ADVISORY COMMITTEE
FOR AERONAUTICS

JAN 26 1954

WASHINGTON
January 20, 1953

1Y

NACA RM E52J31

NATIONAL ADVISORY COMMITTEE FOR AERONAUTICS

RESEARCH MEMORANDUM

EXPERIMENTAL INVESTIGATION OF RADOME ICING AND ICING PROTECTION

By James P. Lewis and Robert J. Blade

2681

SUMMARY

An investigation has been conducted in the NACA Lewis icing research tunnel to determine the icing characteristics, the effects of icing on radar operation, and the protection requirements for two radome configurations. The radomes were for the F-89 airplane and were investigated at airspeeds up to 290 miles per hour, air total temperatures from -15° to +20° F, water contents up to 1.0 gram per cubic meter, and angles of attack of 0° and 4°. A fluid protection system using ethylene glycol was used for both anti-icing and de-icing.

The impingement of water and formation of ice on the radomes were found to agree well with theory and experience. The ice formations were found to produce serious effects on the radar performance. The fluid protection system gave adequate icing protection with anti-icing and de-icing requirements of practical magnitude.

INTRODUCTION

In modern all-weather aircraft, radar has become of increasing importance in assuring successful performance of the airplane in all atmospheric and operational conditions. This is particularly true of military aircraft, where, in addition to its use as a landing and navigational aid, radar is used for bomb sighting, target tracking, and gunfire control. Successful operation of modern aircraft demands, therefore, unimpeded radar operation.

The radome or radar housing serves a dual role, being part of both the radar system and the aircraft structure. As part of the radar system the radome is designed to have the minimum effect on the radar operation; as an airplane component it is subject to normal airplane design problems including that of icing and icing protection. Radomes are normally of such a shape and location on the aircraft that the aerodynamic penalties resulting from icing are usually negligible; the main concern is the preservation of the radar operation. It is of importance, therefore, to know the effect of radome icing on the radar electrical properties. In addition, it is necessary to evaluate the radome icing-protection system as regards both the removal or prevention of ice and any possible effects on radar operation.

At present very little is known of the effect of radome icing on radar operation. Theoretical calculations of the transmission of microwaves through ice can be made but are dependent upon the values assumed for the electrical properties of ice. Reference 1 indicates considerable variation in both the dielectric constant and conductivity for bulk ice produced in the laboratory. In addition, it is known that ice formations encountered in flight are considerably different in type and structure from bulk ice. Flight radome icing very probably would also differ in type and structure from ice produced on a radome in static conditions as in a cold chamber. It would appear, therefore, that neither calculations nor static tests will give realistic values of the effect of radome icing on radar performance.

In order to evaluate the icing and icing protection of radomes, an investigation was conducted in the NACA Lewis laboratory icing research tunnel. The objectives of the investigation were to determine the manner in which the radome collects ice and water, including measurement of both the rate and area of water impingement, the determination of the effects of radome icing on the radar performance, and the evaluation of a method of icing protection for the radome. The radomes investigated were those for the F-89 airplane. Icing protection was achieved by spraying a temperature-depressant fluid on the radome surface.

APPARATUS AND PROCEDURE

Description of Radomes and Radar

Two radome configurations were tested, those for the F-89C and F-89D airplanes employing APG-33 and APG-40 radar, respectively. The radar is of the conical-scan type with a parabolic reflector-type antenna. The radar is mounted in the nose of the airplane; the radomes are bodies of revolution which fair into the nose of the fuselage. Sketches showing sectional views of the two radome configurations are presented in figure 1. The narrow C-radome is essentially parabolic in section having a nose radius of 6.955 inches. The blunt D-radome is almost hemispherical, with a nose radius twice that of the C-radome, or 13.91 inches. Figure 1 also shows the location of the two radomes relative to a common reference plane on the airplane. Both radomes were of similar construction, consisting of molded Fiberglas impregnated with a synthetic resin; the nominal thickness of both radomes was 3/8 inch. The outer surfaces of the radomes were coated with Gayco, a rubber-like material, to resist erosion and abrasion.

The radar operates in the X-band (3.2 cm wavelength) with nominal frequencies of 9245 and 9375 megacycles for the C- and D-radomes, respectively. The operation of this type of radar can best be seen by reference

to figures 2 and 3. The radar feed which projects ahead of the parabolic antenna directs the microwave signal towards the antenna, which reflects the electromagnetic beam forward. Since the feed is rectangular, a beam which is elliptical in cross section is obtained. The antenna nutates about a spin axis and is also set at an angle with respect to the spin axis as shown in figure 2. The radar beam is thus made to follow a wobble motion; the center of the beam describes the surface of a cone in space. In addition, the antenna moves or scans with respect to the radome axis in both the azimuth and elevation planes. Space limitations restricted the scan angle to $\pm 30^{\circ}$ and $\pm 35^{\circ}$ on the C- and D-radomes, respectively. Any object that falls within the beam during a nutation of the antenna will return a series of echos that are amplitude-modulated as the antenna rotates. The modulated signal can then be used to indicate the angular displacement of the line of sight from the antenna to the object relative to the radome axis.

The antenna and necessary electronic equipment together with the test radomes were mounted on a faired afterbody installed in the test section of the icing research tunnel. A view of the setup with the C-radome removed showing the antenna is shown in figure 3. A photograph of the installation with the D-radome is shown in figure 4. The nozzle shown at the nose of the radome is part of the liquid icing-protection system.

Experimental Procedure

The experimental investigation was divided into three phases: (1) determination of the rate and location of water-droplet impingement on the radome and the manner in which the radome iced, (2) measurement of the effect of radome icing on the radar characteristics, including effects on transmission and displacement of the radar beam, and (3) evaluation of the effectiveness of the liquid icing-protection system. The experimental setup and procedure for each phase of the investigation are discussed separately.

Droplet impingement and icing. - The determination of the rate and location of the water-droplet impingement was accomplished by a tracer technique. Small amounts of a water-soluble dye (Azo Rubine) were placed in the icing-cloud spray water which was injected into the tunnel air stream ahead of the test section at air temperatures above freezing. Strips of an absorbent paper were wrapped around the radome surface upon which the water-dye solution impinged during the short (1 to 10 sec) exposure period. The liquid-water content of the cloud during these short exposures was obtained by exposing a narrow strip of the absorbent paper having a high and known collection efficiency. The quantity of dye collected on the absorbent paper was determined by means of a spectrophotometer, which together with the known dye concentration in the spray cloud yielded the local rate of deposition of water on the radome and the

local collection efficiency. Impingement results were obtained for both the C- and D-radomes at airspeeds of approximately 175 and 290 miles per hour, angles of attack of 0° and 4°, liquid-water contents of 0.4 and 1.14 grams per cubic meter, and mean effective droplet diameters of 9 to 14 microns.

Operation of the cloud-spray system at subfreezing air temperatures produced icing of the radomes. The radomes were allowed to ice for periods of 15 minutes, during and after which visual observations and photographs of the ice formations were obtained, together with measurements of the ice thickness at the end of the icing period. Icing of the radomes was obtained at airspeeds of 168 and 275 miles per hour, angles of attack 0° and 4°, air total temperatures of -5° to $+12^{\circ}$ F, liquid-water content of approximately 0.9 gram per cubic meter, and volume-median droplet diameters of approximately 10 to 12 microns.

Effect of icing on radar characteristics. - The tests were conducted as nearly as possible in accordance with the specifications of the Aircraft Industries Association (reference 2), with the recommended klystron signal source in place of the magnetron ordinarily used in aircraft radar. A sketch showing the arrangement of the radome and electrical equipment for the transmission tests is given in figure 5. One-way transmission of the radar beam into the radome was used to isolate the transmission losses from the effects of beam deflection. Conversely, one-way transmission of the beam out of the radome to a target antenna was used in the beam-deflection tests to obtain maximum sensitivity and to isolate as much as possible the effects of transmission. The signal equipment, which consisted of a signal generator (including power supply and modulator) with a 2K39 klystron reflex oscillator having a 250-milliwatt output, was fed from a 115-volt outlet through a constant-voltage transformer to eliminate effects of changes in line voltage. The rest of the transmitting unit included a suitable adapter, attenuator, wave guide, and transmitting antenna. The klystron tube and tuner, adapter, attenuator, and antenna were mounted on the icing-cloud spray-system frame located ahead of the tunnel contraction section. A view of the transmitter mounted on the spray frame is shown in figure 6. The distance between the transmitting and receiving antennas was 39 feet 9 inches.

The receiver section inside the radome was so mounted as to maintain the same location of the antenna with respect to the radome as in the airplane. The receiver, including the receiving antenna and feed, a double-slug tuner, a bolometer detecting section, antenna mount, and drive, was installed on a movable carriage inside the radome. Leads from the detecting section were brought outside the tunnel test section to the bolometer power supply, preamplifier, and amplifier, and then to a polar recorder. The receiving and transmitting antennas were alined for maximum received power. All electrical equipment was allowed sufficient warm-up time; a supply of dry air was used to prevent overheating of the klystron tube. Mounting of the transmitter on the spray frame had no detrimental effects on the spray cloud; the transmitter was adequately shielded from ice and moisture.

[redacted]

With the tunnel inoperative and the radome removed, the system was tuned for 100-percent power transmission. The radome was then installed, and the transmission obtained was checked against values previously measured in dry-air static tests (98 percent for the D-radome and 87 percent for the C-radome at 0° azimuth and elevation). When the desired tunnel airspeed and temperature conditions were reached, the radome was iced for a period of 15 minutes at the specified icing conditions. Transmission measurements were made during the icing period with a relative angle of 0° between the antenna and radome axes in both azimuth and elevation planes. At the end of the icing period the tunnel was further refrigerated to aid in preserving the ice formation. After the tunnel was shut down, the radome was disconnected from the afterbody, and the movable carriage on which the radome and receiving antenna were mounted was pulled forward a sufficient distance to allow the radome to be rotated and pivoted. Transmission measurements were than taken at various scan angles in the azimuth plane. The radome was then rotated 90° in a clockwise direction looking downstream around the longitudinal axis of the model, and transmission measurements at various scan angles were again made. In flight, the antenna scans through an angle range with respect to a fixed radome. In the tunnel tests, however, the radome was pivoted about a fixed antenna to avoid moving the transmitting antenna. With the radome at 0° scan angle with respect to the antenna axis in the azimuth and elevation planes, the radome was rotated around the longitudinal axis of the model a full revolution clockwise looking downstream and a record of the transmission obtained. At one test condition the transmission of the dry radome and the transmission through the spray cloud and wetted radome at air temperatures above freezing with the tunnel operating were also obtained. Frequent checks of the transmission with the radome removed were made during the measurement period.

For the beam-deflection or bore-sight shift measurements, the transmitting and receiving antennas were interchanged and a vacuum-tube voltmeter was substituted for the polar recorder. A sketch of the equipment arrangement for the beam-deflection tests is given in figure 7. The transmitting antenna was offset from its axis of rotation by a cam (see fig. 2), so that by rotating the transmitting antenna the radar beam was made to follow a circular path around the target antenna (polarization was kept horizontal). With no deflection of the beam, there are no differences in readings from the target antenna at rotational positions of the transmitting antenna 180° apart. The system was calibrated in the tunnel (with the radome removed) by displacing the target antenna known distances horizontally in a plane perpendicular to the longitudinal axis of the tunnel and recording the maximum and minimum power values corresponding to 180° rotation of the transmitting antenna. The radome was then installed and iced at the desired conditions for 15 minutes. At the end of the icing period the radome was pivoted through a range of scan angles with the transmitting antenna being rotated at each angular

scan position to obtain the beam shift corresponding to the difference in the maximum and minimum power readings. The radome was then rotated 90° as in the transmission tests, and the beam deflection measurements were repeated.

Fluid-protection system. - The fluid-protection system consisted simply of a spray nozzle located in the radome nose which sprayed a mixture of ethylene glycol and water ahead of the radome; the spray mixture was then swept back on the radome surface by the air stream to remove or prevent ice as desired. A mixture of 60 percent ethylene glycol and 40 percent water by weight was employed as producing the greatest depression in the freezing point. A curve of the freezing point of aqueous ethylene glycol mixtures is given in figure 8. A small amount of a red dye (Azo Rubine) was placed in the glycol fluid mixture to aid in distinguishing the fluid spray from the impinging cloud water and ice. Glycol was chosen as the protective fluid since it is practically nonvolatile and thus avoids the appreciable cooling effects obtained from the evaporation of volatile fluids such as alcohol.

Several different types of spray nozzles were employed in the investigation, including both air-atomizing and fluid-atomizing nozzles. The four types of fluid-atomizing nozzles used are shown in figure 9. Three types of air-atomizing nozzles were used, two of which deflected the fluid, spraying through an annular opening. The third did not deflect the fluid, but sprayed straight ahead. Photographs of air-atomizing nozzles are shown in figure 10. The T364M (shown in fig. 10) and T365M deflecting-type nozzles were essentially the same, the T364M nozzle spraying to the rear at 45° while the T365M nozzle sprayed forward at 45°. A sketch of the installation of the T364M nozzle is shown in figure 11. All nozzles sprayed a hollow-cone pattern. The glycol mixture was fed from a pressurized supply tank through suitable regulator valves and a rotameter. Fluid and air pressures were measured at the nozzle.

The procedure in evaluating the anti-icing performance of the liquid protection system was as follows: After the desired tunnel airspeed and temperature were obtained, the glycol was turned on in sufficient quantity (approximately 40 lb/hr) to flood the radome surface. The icing cloud at the desired density and droplet size was then started. The glycol flow rate was then gradually reduced until a marginal flow rate was obtained, the point at which ice particles were observed to begin forming and remaining on the radome surface. For the air-atomizing nozzles, tests were made at various nozzle air pressures. Visual observations and photographs were made during this evaluation process.

For the case of de-icing, the radome was allowed to ice for a specified period at the desired speed, temperature, and icing conditions. The glycol spray was then turned on at an arbitrary value of flow rate and pressure while the icing cloud continued to impinge on the surface. The time and manner of de-icing were recorded by photographs and visual observations.

RESULTS AND DISCUSSION

The results of the investigation are discussed separately in terms of the radome icing characteristics, including water-droplet impingement and type of icing, the effects of icing on the radar characteristics, and the evaluation of the fluid-protection system.

Icing Characteristics

Results obtained by the tracer technique for the impingement characteristics of the two radome configurations showed both the rate and location of deposition of the cloud water on the radome surface. Typical ice formations were also obtained at various icing, speed, and temperature conditions.

Water-droplet impingement. - The cloud obtained in the tunnel contained water droplets of various diameters. The size distribution obtained is given in figure 12 in terms of the volume-median droplet diameter d_o, which is defined as the diameter for which half the cloud water volume is contained in droplets less than the median and half of the water volume is in droplets greater than the median. The droplet-size distribution obtained in the tunnel is fairly close to the type C and D distributions of reference 3.

The results of the investigation of water-droplet impingement on the radome are presented in figures 13 and 14 for the two radome configurations at two angles of attack. The distribution of the impinging water on the surface is given in terms of the local impingement efficiency β, which is the ratio of the amount of water impinging on a differential area of the radome to the maximum water that could impinge on this local area of the radome if all the droplet trajectories were parallel to one another and to the undisturbed air streamlines and if the surface area were projected into a plane perpendicular to the trajectories. The local rate of water interception may be obtained by multiplying the β values by the cloud liquid-water content and airspeed. The total rate of water intercepted by the radome is obtained by integrating the local rate of interception over the entire wetted area of the radome.

In general, all the curves of water interception show the same relations. The curves for zero angle of attack are, of course, symmetrical about the radome nose. At an angle of attack of 4° the peak rate of interception is shifted approximately 1 to 2 inches away from the nose, but the curves are still approximately symmetrical around the location of the peak value. Aft of the peak point the curves decrease approximately linearly to a β value of about 1 to 2 percent, where they bend sharply, indicating a relatively large area of the radome collecting very small amounts of water.

The distribution of impingement with surface distance from the radome nose decreases much more sharply on the C-radome than on the D configuration, but the C-radome has a greater rate of impingement in the nose area. At 4° angle of attack the C-radome shows a smaller variation in the location of the peak impingement point than does the D-radome. A comparison of the impingement on the two radomes at the same speed and droplet-size conditions is given in figure 15, together with a comparison of the experimental results with the theoretical values of Langmuir (reference 3) for impingement on spheres. The theoretical curves were obtained by weighting the data of Langmuir for single droplet sizes in accordance with the experimental cloud droplet-size distribution of figure 12. Fairly good agreement of the local impingement efficiencies is obtained, especially for the C-radome.

A total collection efficiency E_m of water interception may be defined as the ratio of the actual total amount of water impinging on the radome to the maximum amount of water that could impinge on the model. This maximum catch is the amount of water that would impinge on the radome model including the model afterbody if there were no deflection of the water droplets:

$$E_m = \frac{M}{0.3296\ mVA}$$

where

E_m total collection efficiency

M total rate of water intercepted, lb/hr

m cloud liquid-water content, g/cu m

V airspeed, mph

A projected area, sq ft, corresponding to maximum diameter of radome model afterbody, 3.19 ft

An equivalent sphere collection efficiency may also be defined in which the area used in the denominator of the efficiency term is the area of a circle with a radius equal to that of the radome nose radius (fig. 1). The experimentally determined collection efficiencies at various airspeed, droplet-size, and angle-of-attack conditions is given in the following table:

Radome type	Airspeed V (mph)	Volume-median droplet diameter d_o (microns)	Angle of attack (deg)	Experimental collection efficiency (percent)	
				Equivalent sphere efficiency (Based on nose radius)	Total efficiency E_m (Based on model maximum radius)
C	176	11	0	1.7	0.23
	179	14	0	4.4	.58
	286	9	0	2.9	.38
	288	12	0	5.9	.78
	174	11	4	1.5	.2
	176	14	4	3.9	.51
	288	9	4	2.5	.33
	290	12	4	4.7	.62
D	176	11	0	0.4	0.19
	176	14	0	1.4	.7
	290	9	0	.7	.39
	177	11	4	.3	.14
	176	14	4	1.1	.58
	290	9	4	.7	.35
	289	12	4	1.9	.97

Radome icing characteristics. - The results of a study of typical radome icing are presented in the photographs of figures 16 and 17 for the C- and D-radomes, respectively. The photographs of figure 16 indicate that the main ice formation on the C-radome is confined to a rather narrow region near the radome nose. These main formations extend rearward a distance of 6 to 8 inches and are followed by a very light frost-like formation that extends to the rear of the radome. The relatively small area of the main ice formation agrees with the result of figure 13, which showed most of the water impinging in an area 4 to 6 inches from the radome nose at zero angle of attack together with a sharp decrease in the local collection efficiency aft of the nose. Considerable differences in the type of ice on the C-radome result from variations in airspeed, temperature, and rate of impingement. Figure 16(a) indicates a dark area approximately 2 inches in diameter. This dark area does not indicate the absence of ice but that the ice present is of a glaze, transparent type. This glaze area was approximately 5/16 inch thick and was followed by a rough formation of opaque (or rime) ice in the form of overlapping feathers. This glaze formation at the nose results from a combination of effects of air temperature, airspeed, collection rate, and droplet size. At the low airspeeds, a large percentage of the water impinging upon the nose area is in the form of relatively large droplets which break and form a film of water before freezing and thus entrap little or no air. In addition, the nose area

[redacted]

has the greatest temperature recovery and the greatest rate of impingement, thus producing a relatively large release of heat of fusion. All these effects combine to prevent instantaneous freezing of the droplets upon contact and the subsequent entrainment of air that produces the opaque rime formation. In figure 16(b) the nose formation is a semi-rime 3/4 inch thick. The formation of figure 16(c), which was obtained at the same airspeed but slightly higher air temperature and water content than figure 16(b), has a semiglaze formation at the nose. In figure 16(d) the dark area at the nose has entirely disappeared, a pure rime formation being obtained.

The results of icing of the D-radome (fig. 17) show the same general types of formations as for the C-radome. The main ice formation is spread over a greater area, has a more gradual change in thickness, and in general is slightly rougher than that of the C-radome. The main ice formation was followed by the characteristic frost-like formation. This frost-like ice is believed to be the result of a secondary turbulent deposit of very small droplets caused by the presence of the main ice formation on the nose of the radome. The ice formations on the D-radome were more glaze-like than for the C-radome at similar conditions. This result is to be expected as the larger and blunter D-radome will deflect a greater percentage of the small droplets that produce rime formations than the smaller sharper-nosed C-radome.

The formations on both radomes were very rough, porous, and of varying kinds of ice. Such ice formations will probably have considerable variation in their properties, especially the electrical conductivity and dielectric constant, and hence wide variation in their effect on radar transmission. Dorsey (reference 1) indicates considerable variation in the electrical properties of solid ice made in the laboratory; and the rough, irregular formations obtained on the radomes would be expected to exhibit an even greater range of electrical properties.

It should be emphasized that the results of both the water-impingement and icing studies are strictly applicable to the radome and afterbody shapes tested and for the specific droplet-size conditions obtained in the tunnel. The droplet-size distribution obtained in the tunnel, however, is felt to be fairly representative of natural conditions, and the impingement and icing results should be very close to those obtained in flight. For most design purposes, interpolation of the impingement results reported herein should yield values of sufficient accuracy for similarly shaped bodies. In addition, the fairly close agreement of the experimental and theoretical results (fig. 15) indicate that the sphere values may be used especially for the case of different droplet-size distributions. Design values so obtained should have an accuracy comparable with that with which the cloud liquid-water content is known.

Effect of Icing on Radar Characteristics

The effects of icing on the radar performance were investigated in terms of the loss in energy transmitted and the deflection of the radar beam. Results showing these effects are presented for several icing, temperature, and airspeed conditions.

Effect on transmission. - Previous to the investigation of the effects of ice on transmission, a few checks were made to determine the effects of operation of the tunnel and the spray cloud at air temperatures above freezing on the radome transmission characteristics. With the tunnel operating at an airspeed of 275 miles per hour, air temperature of 29° F, and no spray cloud, transmission through the D-radome at 0° in the azimuth and elevation planes showed approximately a 2-percent reduction from that with the radome removed. At the same airspeed, a liquid-water content of approximately 0.8 gram per cubic meter, and volume-median droplet diameter of approximately 12 microns at an air temperature above freezing, a reduction in one-way transmission through the D-radome up to 5 percent was obtained. It is believed that this loss is caused almost entirely by the water film on the radome surface rather than by the droplets in the cloud. Unpublished calculations and flight experience indicate that for 3-centimeter radar, both droplets and distances through a cloud larger than those employed in the icing tunnel investigation would be required at normal water contents to produce measurable losses in transmission. The water film on the radome surface was very thin, and the water was carried off by the air stream almost as fast as it impinged. Because of this thin water film, the transmission losses were relatively small as compared with the large values that have been obtained in static tests where large amounts of water were sprayed on the radome. Unpublished data for such tests have indicated transmission losses up to 85 percent.

Transmission measurements were made during the 15-minute period in which the radomes were iced. These results are presented in figure 18 for the two radomes at zero scan angle and zero angle of attack. A theoretical curve has also been plotted for comparison with the experimental values. This theoretical curve was computed from the equations of reference 4 for normal one-way transmission through a flat plate of ice increasing in thickness at the rate of 2 inches per hour. A dielectric constant for ice of 3.3 and a loss factor of 1.66×10^{-6} (defined as electrical conductivity of material divided by product of frequency and dielectric constant) were assumed. All the experimental curves tend to oscillate as does the theoretical curve; this effect is more pronounced for the D- than for the C-radome. This result should be expected, since, as the ice thickness increases in multiples of the wavelength, alternate reinforcing and cancellation effects will occur as the wave is reflected in its passage through the ice layer. The average rate of decrease in transmission and the average rate of ice deposition at the radome nose is given for the experimental results in the following table:

Radome type	Airspeed (mph)	Air total temperature (°F)	Average rate of decrease in transmission (percent/min)	Average rate of ice accretion at nose (in./hr)
D	274	12	2.8	1.5
D	275	-4	3.5	2.0
C	273	-5	4.2	3.0
C	168	10	2.2	1.25

Although these data are rather limited, they indicate that the decrease in transmission is primarily a function of ice thickness; the variations in the type of ice appear to be of second-order importance. The narrow C-radome shows the greatest rate of decrease in transmission, primarily because of its greater ice accretion rate.

At the end of the icing period, transmission measurements were made in the inoperative tunnel at various scan angles. These results for the two radomes are presented in figures 19 and 20. After measurements were made through a range of scan angles with the radome in its original position relative to its rotational axes, the radome was rotated 90° around its axis and the measurements were repeated. The directions left and right and up and down are measured looking upstream and refer to the sector of the radome through which the beam scans. Two different curves were thus obtained, because, as indicated in the photographs of figures 16 and 17, the ice formations were unsymmetrical and the radar beam was elliptical in cross section with its major axis oriented in the azimuth plane. Values of the dry radome transmission are also plotted. The curves of transmission efficiency for the two radomes differ both in magnitude and shape. The dry curve for the C-radome shows a depression at 0° scan angle, while the transmission through the D-radome is constant at 98 percent. The experimental curves for the C-radome also show the greatest transmission loss near 0° scan angle, in contrast to the curves for the D-radome, which are either flat or peak near 0° scan angle. Aside from the electrical properties of the dry radomes, the shape of the transmission curves depends primarily on the respective ice formations. As previously shown, the narrow C-radome had the greatest rate of ice accretion, the ice formations were confined to a relatively small area near the nose, and the formations decreased fairly rapidly in thickness with increasing distance from the nose. Thus the C-radome shows the smallest transmission efficiency (10 percent) through the nose area, and as the beam moves away from the nose it passes through a region where the ice thickness decreases rapidly and the transmission efficiency correspondingly increases sharply. In contrast, the ice formations on the blunt D-radome are less in thickness than for the C-radome, cover a greater area, and have a more gradual change in thickness. On the D-radome, therefore, as the beam sweeps through an angle, it still passes

[redacted]

through an ice formation of approximately the same thickness, and only gradual changes in transmission result. In considering the effect of icing on the radar transmission, attention should be given not only to the ice thickness but also to the type of ice and the iced area relative to the size and shape of the radar beam. The size of the antennas produces beams that, in cross section, are of the same approximate size as the projected area of the radome covered by ice. Thus at any one scan angle the transmitted microwave energy is an integration over an area varying in both ice thickness and type.

The curves of figures 19 and 20 show the effect of the unsymmetrical ice formation producing differences in transmission efficiency at two rotational positions of the radome at various scan angles. Additional results of this nature are shown in figure 21. For these data a continuous record of the radar transmission was obtained while the radome was rotated a complete revolution around the longitudinal axis of the model at 0° scan angle. For these particular tests, asymmetric ice formations on the radomes were obtained which resulted in a variation of over 20 percent in transmission efficiency. Although no data on transmission were obtained with an iced radome at an angle of attack to the air stream, the data of figure 21 give an idea of the results that might be obtained at such a condition. As indicated in figures 13 and 16(d) the ice formation at angle of attack is very similar to that at 0° except that it is not centered around the radome nose but is asymmetrical with respect to the longitudinal axis of the radome. Thus the transmission efficiency through such ice formations would vary similarly, although probably to a greater degree, to the results of figure 21.

All the transmission results show rather large effects of icing on the radar transmission. Serious losses in transmission efficiency can result after only short icing exposures. The minimum allowable average transmission efficiency specified by the aircraft manufacturer for the D-radome is 90 percent. Efficiencies less than this were obtained within only 5 minutes of icing with ice formations as small as 1/8 inch thick. In general, all the results indicate ice thickness and radome geometry to be the prime factors affecting the transmission through an iced radome. Airspeed, temperature, and type of ice are of second-order importance; but their exact effects are difficult to evaluate with the limited data available. At higher airspeeds, the loss in transmission should be greater because of the greater rate of ice accretion and hence ice thickness.

Beam deflection. - In addition to the reduction in transmission, another effect of ice on radar performance is the deflection or shifting of the radar beam. This deflection is caused by refractive effects as the beam passes through an asymmetric formation or one of varying thickness or type of ice. This effect is important in the case of tracking or gunfire control, in that an erroneous angle and rate of change of

[redacted]

angle is reported between the search vehicle and the target. Limited measurements of the effect of radome icing on beam deflection made in the icing tunnel investigation are presented in figure 22. All directions are taken looking upstream. As for the case of transmission efficiency, measurements were made with the radome in its normal position and after being rotated 90°. The beam deflection has components in both the azimuth and elevation planes. Time limitations, however, prevented the obtaining of deflection measurements in the vertical direction. Results are presented for the C-radome only; the beam deflection for the blunt D-radome would probably be less, since the ice formation is thinner and of a more uniform thickness. The data of figure 22 are very similar for the two radome positions, especially as to the slope of the curve between the two peak values. The greatest beam deflection obtained was 13.5 mils, and the slopes of the deflection curves between the peak values were 0.83 and 0.75 mil per degree for the normal and 90° positions, respectively. The shape of the deflection curves is such that the beam is bent inwards towards the longitudinal axis of the radome or line of flight; that is, when the beam scans to the right it is bent to the left, and vice versa.

The type and conditions of the icing tunnel tests as well as time limitations prevented both the attainment of high accuracy in the experimental measurements and quantitative evaluation of all the errors of measurement. Inaccuracies in the transmission measurements include those caused by drift in the klystron tube and recorder, the linearity response of the recorder and amplifier, reflections from the tunnel side walls, and temperature effects on the bolometer detecting element. Most of these errors, especially the linearity response, temperature effects, and beam-deflection effects, are considered to be very small. The drift error was compensated for by rechecking the gain setting during the tests. An additional possible source of error for the beam-deflection tests was the nonuniformity of transmission through the iced radome. The calibration used in the beam-deflection measurements was based on the assumption of uniform power attenuation throughout the entire area covered by the beam. This condition is, of course, not fulfilled when the beam is passing through an ice formation of nonuniform thickness, as evidenced by the transmission results. Evaluation of the error introduced by this effect is complicated by the fact that the power readings of the target antenna represent an integration over some portion of a beam the actual geometric location and local attenuation distribution of which is unknown. The direction of the apparent beam deflection caused by the type of variation in transmission efficiency as shown in figure 19(a) for the C-radome is such that the true beam deflection would be less than that indicated in figure 22. For the D-radome, the effect of the variation in transmission efficiency as shown in figure 20(b) is such that the true beam deflection would be greater than the apparent beam deflection.

Evaluation of the seriousness of the effects of icing of radomes is difficult because of the many unknown and variable factors involved. The importance of radome icing will depend upon the type of radar, its location, use, the aircraft itself including its specified mission and performance, and any auxiliary equipment controlled or connected with the radar. Strictly speaking, the one-way laboratory-transmission and beam-deflection tests may be compared only with similar tests on dry radomes. The results are, however, a measure of the effect of radome icing on actual radar operation in flight. The effect of loss in transmission is of importance as affecting the useful range of the radar and may render objects indistinct on the radar screen or make the gunfire control servomechanism insensitive or erratic because of electrical noise. The beam deflection is of importance in the case of tracking or gunfire control, especially when the information is fed into a computer. To determine the effects of beam deflection on, for example, the distance by which a projectile fired from an interceptor will miss its target, it is necessary to know rate of change of the beam-deflection error, the speeds and relative paths of the target, interceptor, and projectile, the range, and the time of firing as well as the instantaneous beam-deflection error. The rate of change of beam-deflection error is of importance in that it reports a false target velocity resulting in an erroneous rate of closure on the target. To the error or miss distance from this source must be added or subtracted the error in target position resulting from the instantaneous beam-deflection error at the time of firing. Both the beam-deflection and transmission-efficiency data indicated that the greatest effect of radome icing occurs in the area included by scan angles up to approximately 30°, which includes the critical region for most gunfire control and missile guidance systems. Losses in transmission and beam deflection from icing were obtained that exceeded the allowable limits for the radomes investigated. Significant losses in transmission were obtained with ice formations at the radome nose less than 1/8 inch thick.

In addition to the loss in transmission efficiency and beam deflection, there may be other important factors affected by radome icing which were not specifically measured. These include polarization, reflection, increase of the side lobes, and any effects that would arise in flight from the use of the normal high-power magnetron tube instead of the low-power klystron tube used in the icing tunnel tests. Polarization effects are complicated, because they are different in the elevation and azimuth scan planes. Even small reflections back into the transmitting antenna could make large differences in the load impedance presented to the transmitter, and may cause frequency pulling or complete stoppage of oscillation. Frequency pulling is of importance in that it can not only result in loss of power output but, more seriously, cause the transmitter to be out of tune with the receiver. Multiple reflections will tend to raise the side lobe level and shift the radar beam. Application of low-power, one-way laboratory tests to flight conditions has certain inherent limitations, and the introduction of icing conditions makes the evaluation of the test data even more difficult.

[redacted]

In general, the results of the investigation indicate that radome icing has serious and in some cases prohibitive effects on radar operation, and that means of icing protection are necessary.

Fluid-Protection System

In the evaluation of the fluid-protection system both the anti-icing and de-icing characteristics of the system were investigated. No measurements of the effects of ice, water, or glycol films on radar performance were made during these tests because of limitations of time and of the setup. Unpublished data supplied by the aircraft manufacturer indicate that the fluid-protection system, including the nozzle, had no significant effect on the radar performance. Most of the evaluation of the fluid-protection system was performed with the D-radome, because its simpler and more fundamental shape made the results of more general application.

Anti-icing. - The anti-icing performance of the fluid-protection system was investigated with several different type nozzles. The anti-icing performance was evaluated on the basis of the minimum flow of the glycol mixture required to just prevent icing of the radome, maintaining a running wet surface. No special instrumentation was used; the minimum-flow point being determined by visual observations. The results are presented in photographs of the glycol spray and radome and in terms of the fluid-flow requirement as a function of the icing, airspeed, and temperature conditions.

In general, the performance of the fluid-atomizing nozzles shown in figure 9 was fairly similar. All these nozzles sprayed the glycol mixture a relatively large distance ahead of the radome. For this reason the glycol spray was easily influenced by the air stream; even at small angles of attack most of the glycol spray would be swept away from the radome, with large areas of the radome unprotected even at large flow rates. The Monarch nozzle (fig. 9) produced a very narrow spray cone with relatively little atomization. An angle of attack as small as 0.5° was sufficient to deflect most of the glycol away from the radome surface. The 1/4 LNN4 nozzle produced better atomization but poor performance at angle of attack and required large fluid flows, over 3 gallons per hour at 275 miles per hour, -10° F air temperature, water content of 0.8 gram per cubic meter, and 0° angle of attack. At the same conditions, the 1/4 LNN4W (which is similar to the 1/4 LNN4 nozzle but with a wider cone angle) gave better performance, requiring approximately 2 gallons per hour and performing well at angles of attack up to 2°. At similar conditions, the J318D nozzle indicated anti-icing obtainable at a flow of approximately $1\frac{1}{2}$ gallons per hour; the erratic and irregular distribution of the glycol on the radome surface made determination of

this value difficult and inexact. The forward-spray non-deflecting air-atomizing nozzle shown in figure 10 had, in general, a performance similar to that of the fluid-spray nozzles, being very sensitive to the angle of the air stream.

The two deflecting air-atomizing nozzles (T364M and T365M, figs. 10 and 11) gave the best anti-icing results both as to the amount of glycol flow required and the distribution of fluid on the surface. The rearward spray T364M nozzle gave the better performance over the range of conditions tested, but the forward-spraying T365M nozzle was slightly superior at angle of attack. Views of the spray cone and flow of fluid on the radome surface produced by the T364M nozzle are shown in figure 23. The two views of figure 23(a) and 23(b) show the spray cone with an excess flow of fluid on the radome surface. The glycol flow rate is approximately 2 gallons per hour with no cloud-water spray. Reducing the flow rate slightly produces the partially wetted surface of figure 23(c), although the full spray cone is maintained. Further reductions in the glycol flow rate result in less of the radome being wetted with the flow in the form of streaks or rivulets. Eventually a point is reached at which the spray cone breaks down, and the fluid flows back over the nozzle and produces a very uneven distribution on the radome.

The photographs of figure 24 show some typical results of anti-icing on the D-radome with the T364M nozzle. In figure 24(a) insufficient fluid is supplied and the ice is building up on the front of the radome. Increasing the flow rate to 11 pounds per hour (fig. 24(b)) eliminates the ice at the radome nose, but large slush-like formations appear at the rear of the radome. At a flow rate of 12.5 pounds per hour (fig. 24(c)), the radome is entirely free from ice, although runback icing of a slush type occurs on the afterbody. Figures 24(c) and 24(d) show the fluid and runback ice formations remaining on the afterbody after the 34 minute test run. The large amounts of fluid and ice on the afterbody indicate the possibility of obscuring the aircraft windshield with this type of system.

Typical photographs of the radomes with the T364M nozzle at the marginal anti-icing point are shown in figure 25 for various conditions. At the high air temperature and low glycol flow conditions (figs. 25(a), (b), and (c)) the glycol-water flow over a large part of the radome is in the form of rivulets. Despite the fact that only part of the radome surface is wet by the glycol, no ice builds up between rivulets. Sufficient glycol was deposited in the region of direct cloud-water impingement to prevent freezing, the impinging water and the glycol mixture then combining to flow rearward in common rivulets. At the low air temperature and higher glycol flow rates (figs. 25(d) and (e)), practically all of the surface is wet. At these conditions, the fluid flow on the surface exhibited a grainy appearance caused by the presence of large drops of water and small particles of ice in the fluid film, although no

[redacted]

ice adhered to the radome surface. For this reason, the glycol flow requirements presented herein should be regarded as minimum values and should be increased slightly for practical application. The data of figure 25 show an increase in the flow requirements with decrease in air temperature. The requirement for the C-radome at 10° F is approximately half that for the D-radome. Approximately the same amount of water is intercepted by the two radomes, and the deposition efficiency (defined as the ratio of amount of fluid striking radome to amount of fluid sprayed) of the glycol spray is slightly greater for the D- than for the C-radome. The lower fluid requirement for the C-radome appears, therefore, to result from a better distribution of deposition of the fluid mixture on the C-radome relative to the distribution of water impingement; that is, just sufficient fluid is received at each point on the C-radome to prevent freezing, while on the D-radome excess fluid is deposited in some regions in order to obtain sufficient fluid deposition at other areas.

The variation of the fluid anti-icing requirement shown in figure 26 is essentially linear with the cloud liquid-water content. This relation is as expected, since the efficiency of impingement of the cloud water is independent of the liquid-water content, and, for the speed and fluid-flow conditions of interest, the glycol deposition efficiency changes only slightly with increase in fluid flow. The theoretical curve was obtained from the relation of the freezing point of aqueous solutions of ethylene glycol and by making the assumptions (1) that the water catch on the radome can be calculated from Langmuir's theoretical values for a sphere having a radius equal to the nose radius of the radome and (2) that the radome surface temperature is equal to the tunnel air total temperature less 20 percent of the dry kinetic rise. These assumptions are fairly valid, since it was previously shown that the water catch on the radome is closely approximated by the catch on equivalent spheres; and, since the glycol is practically nonvolatile, evaporation will cause only a small temperature depression, especially at the low air temperatures employed. In addition, protection is required over an area of varying temperature and heat-transfer coefficient. Lack of accurate knowledge of local heat-transfer coefficient and the distribution of glycol on the radome surface preclude accurate and detailed computations of the theoretical fluid requirement. Based on the theoretical value given, the system efficiency (defined as ratio of experimental marginal fluid requirement for anti-icing to theoretical requirement) is approximately 76 percent for the conditions of figure 26. Nonicing tests made by the aircraft manufacturer indicated a deposition efficiency of the glycol of approximately 50 percent. The increased system efficiency of the experimental data results from the glycol-impingement distribution; an excess of glycol is deposited at the nose and runs back to an area receiving insufficient glycol by direct impingement.

[redacted]

The fluid anti-icing requirement as a function of air temperature for the T364M nozzle is shown in figure 27. The anti-icing requirement is presented in terms of the ratio of the experimental value of the amount of glycol mixture required for anti-icing to the amount of cloud water intercepted by the radome. The amount of cloud water intercepted was computed from the radome collection efficiency interpolated from the results of the dye tests and the given conditions of airspeed, droplet size, and water content. The theoretical curve was obtained in the same manner as that of figure 26. Considerable scatter of the data is obtained primarily because of the inaccuracy with which the fluid requirement was determined and the inaccuracy of the computation of the amount of water intercepted. Limitations in the accuracy and extent of the data prevent any correlation of the results on the basis of the nozzle air pressure. Over the temperature range shown, the system efficiency varied from approximately 68 to 86 percent. The scatter of the experimental data and the efficiency of the system shown by figure 27 indicate that until more precise data are obtained for the glycol deposition efficiency and distribution, sufficient accuracy in computing the water deposition on the radome may be obtained by use of the data of this report or from equivalent sphere data.

The effect of angle of attack on the fluid anti-icing requirement is shown by the results of figure 28. These data, obtained with the reverse-flow T364M nozzle, indicate a large increase in the anti-icing requirement for angles greater than 2°. The effect of angle of attack is twofold: on the side of the radome turned into the wind the water deposition is increased with less water deposited on the opposite side; while for the glycol spray most of the fluid is directed by the air stream towards the side away from the air stream. These opposing effects result in the rapid increase in the flow requirement at angle of attack. A decrease in the flow requirement at angle of attack might be obtained by placing the spray nozzle closer to the radome surface, thus making it less subject to deflection by the air stream. Both the C- and D-radomes show the same increase in fluid requirement with angle of attack, but the requirements for the C-radome are less than for the D-radome. As might be expected from the sensitivity of the glycol spray to deflection by the air stream, airspeed has an important effect on the anti-icing requirements at angle of attack. Increasing the airspeed from 230 to 275 miles per hour almost doubles the requirement for the D-radome.

The variation of fluid anti-icing requirement for the D-radome with airspeed is shown in figure 29 for two angle-of-attack and air-temperature conditions. These data have been weighted in accordance with the results of figures 26 and 27 in order to compensate for small variations in liquid-water content and air temperature. Both curves tend to approach zero anti-icing requirement at a finite velocity. Theoretical studies indicate that there is some combination of velocity and droplet size at which no cloud water will be deposited on the radome. Lack of accurate and detailed knowledge of the dynamics of impingement

[redacted]

on the specific radomes prevents exact specification of this cut-off velocity. The increase in fluid requirement with angle of attack shown in figure 28 is again apparent. At zero angle of attack, the effect of increase in airspeed is primarily to increase the amount of water caught, which is a direct function of airspeed and collection efficiency, which in turn is a function of airspeed. Increasing airspeed also increases the glycol deposition efficiency and in addition increases the heat-transfer coefficient, thus causing a greater surface-temperature depression. The data of figure 29, however, are presented for constant air total temperature and there is little change in surface temperature with airspeed, a result of the increased kinetic temperature recovery. Most of these second-order effects appear to cancel one another at zero angle of attack, the fluid requirement varying almost directly with airspeed. The marked increase in requirement at angle of attack results primarily from the deflection of the glycol spray rather than from velocity effects on the rate of water impingement.

Extrapolation of these results to higher velocities would appear possible if proper consideration is given to the effects of velocity on the rate of water impingement, surface temperature, and evaporation effects. Greater knowledge is needed as to the deposition characteristics of the glycol spray nozzle, particularly at the higher speeds and for other nozzle and radome configurations.

De-icing. - The de-icing or ice-removal performance of the glycol-protection system for the D-radome and the T364M nozzle is shown in figures 30 to 33. The radome was iced for arbitrary periods before the glycol spray was turned on in order to obtain representative ice formations of a size which, on the basis of the transmission and beam-deflection tests, would have a significant effect on the radar performance. The glycol flow rates were arbitrarily set at values approximately equal to or greater than the anti-icing flow rates at corresponding icing, airspeed, and temperature conditions. The cloud spray was continued during the de-icing period.

Typical de-icing results at zero angle of attack are shown in the photographs of figure 30. Following the icing period, the glycol spray quickly covered and penetrated the ice formation; the dark areas in the photographs show the presence of the red-dyed glycol. The de-icing process is seen to be primarily a washing mechanism, the glycol eroding the formation and breaking it up into sections. The fluid penetrates into and around the ice formation until it is loosened from the surface and slides to the rear of the radome. De-icing for the conditions of figure 30 was completed in $4\frac{1}{2}$ minutes, after which the radome was fully protected by anti-icing. Following stopping of the cloud and glycol sprays, the radome surface was cleaned off quickly by the air stream.

The results of figure 31 at 2° angle of attack show the effect of angle of attack on the glycol spray. The angle of attack is such that the radome nose is displaced away from the camera and the glycol spray is directed towards the far side. Practically all the ice formation is wetted by the glycol within 30 seconds, after which the erosion process continues with most of the ice being first cleaned off the far side and very little glycol flow occurring on the near side. De-icing of the entire radome was completed in approximately $3\frac{1}{2}$ minutes.

Raising the angle of attack to 4° at an airspeed of 171 miles per hour produced the results of figure 32. Again the displacement of the glycol spray is clearly shown; the far side of the radome was completely de-iced in 1 minute. The remainder of the de-icing period was required to de-ice the near side of the radome. After 5 minutes of de-icing, slight amounts of slush remained at the aft end of the radome. Increasing the airspeed to 283 miles per hour at 4° angle of attack (fig. 33) required a fourfold increase in the glycol-water flow rate to obtain similar de-icing performance at approximately the same icing and temperature conditions.

The de-icing performance in general was positive and complete for all conditions investigated. Once the ice formations were loosened from the radome surface, they slid aft and were either carried off by the air forces or continued moving to the rear of the model. The ice usually was either completely melted or formed a slush with the glycol by the time it reached the rear of the radome. Once the radome was cleared and the cloud and glycol sprays turned off, there was at no time any noticeable residue on the radome surface. De-icing tests were confined to the T-364M and T-365M nozzles. Generally the rearward-facing T364M nozzle gave the best performance, the forward-facing T365M nozzle appearing to be effective primarily at angle of attack.

SUMMARY OF RESULTS AND CONCLUSIONS

From the investigation of the icing and icing protection of the F-89 radomes the following results and conclusions are summarized:

1. The impingement and icing characteristics of the radomes were determined for a range of operating and icing conditions. The water-droplet collection efficiency of both radomes was found to be relatively low (0.19 to 0.97 percent, based on maximum radius of the model). The experimental impingement characteristics were found to be fairly close to those computed for spheres from theoretical data. The extent of impingement was sufficiently large to cover most of the radome area scanned by the radar beam during normal operation. The ice formations obtained were typical of those for similar bodies and icing and flight conditions. The icing rate at the radome nose varied from $1\frac{1}{4}$ to 3 inches per hour for the range of conditions tested.

[redacted]

2. Radome icing was found to have a serious effect on the radar operation. Significant losses in transmission were obtained with ice formations as small as 1/8 inch thick and for icing periods less than 5 minutes. Relatively large effects of ice on the deflection of the radar beam were also obtained; for the test conditions the allowable limits for beam deflection were exceeded. From the investigation it is concluded that the thickness of ice, its relative location of the radome, and the radome geometry are the prime factors determining the effects of radome icing on radar operation. It would appear that extrapolation of the transmission results to higher speeds may thus be made on the basis of the ice thickness and orientation. In evaluating radar performance in flight icing conditions, consideration also should be given to the effects of radome icing that were not specifically determined in the icing tunnel investigation.

3. The fluid-protection system was found to provide satisfactory anti- and de-icing performance over the range of test conditions. For anti-icing, fluid requirements of less than 3 gallons per hour of the water-glycol mixture were obtained. The fluid requirements for anti-icing appeared to be primarily a function of rate of water catch, airspeed, and air temperature. Satisfactory de-icing of the radomes was obtained with flow rates less than 4 gallons per hour and for de-icing periods less than 5 minutes. Both the anti- and de-icing requirements were extremely sensitive to the angle of attack of the radome. Satisfactory protection could be achieved only with the deflecting-type nozzle.

Lewis Flight Propulsion Laboratory
National Advisory Committee for Aeronautics
Cleveland, Ohio

REFERENCES

1. Dorsey, N. Ernest: Properties of Ordinary Water-Substance. Reinhold Pub. Corp. (New York), 1940, pp. 445-510.

2. Anon.: Electrical Test Procedures for Radomes and Radome Materials. ATC Rep. No. ARTC-4, Aircraft Industries Association, Washington (D.C.), Dec. 1, 1951.

3. Langmuir, Irving, and Blodgett, Katherine B.: A Mathematical Investigation of Water Droplet Trajectories. Tech. Rep. No. 5418, Air Materiel Command, AAF, Feb. 19, 1946. (Contract No. W-33-038-ac-9151 with General Electric Co.)

4. Anon.: Radome Engineering Manual. AMC Manual No. 80-4, Chief of Bur. Aero. and Commanding General AMC, Oct. 1, 1948. (NAVAER 16-45-502.)

[redacted]

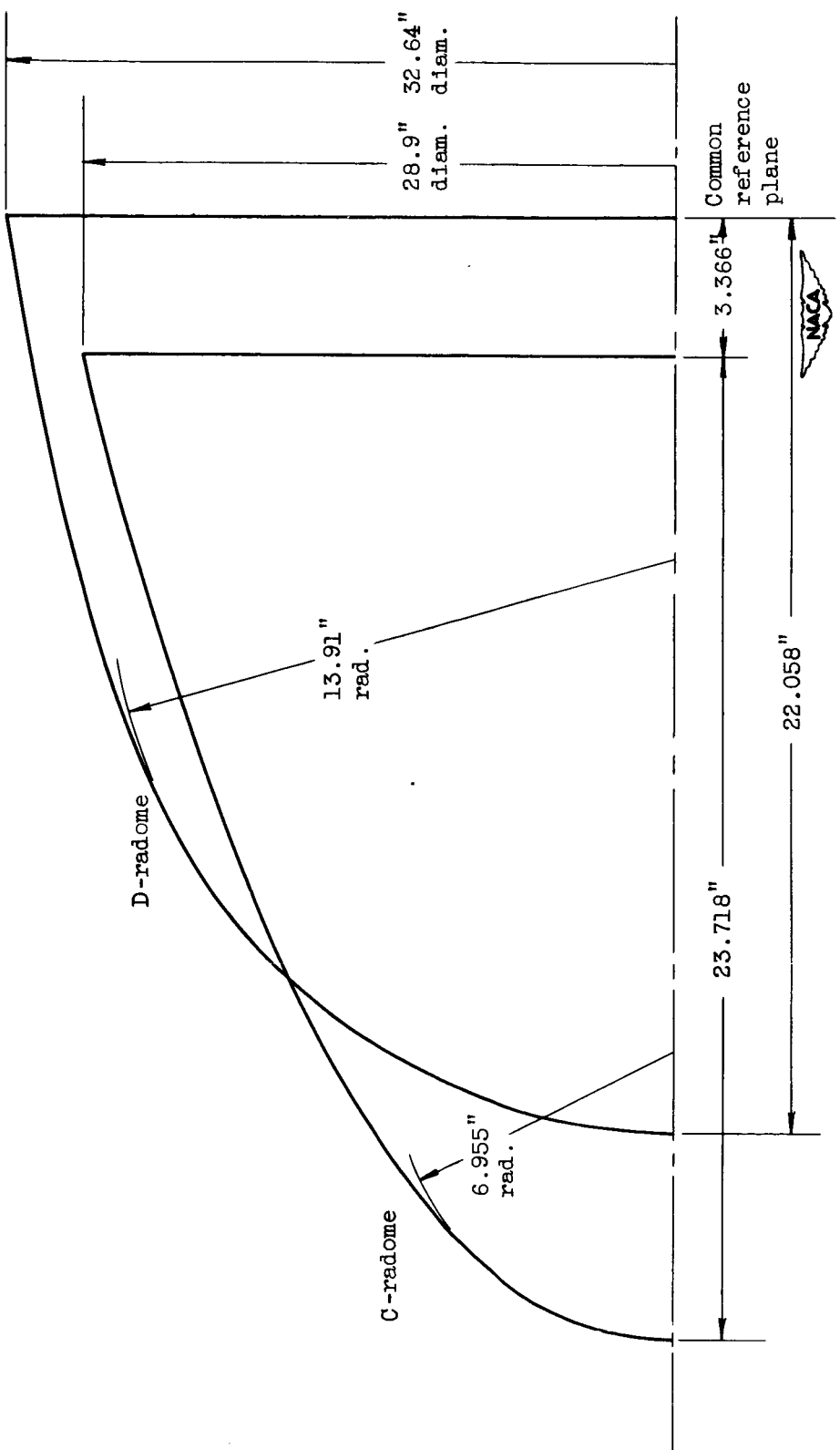

Figure 1. - Sketch showing halfsections of test radomes and relative positions on airplane.

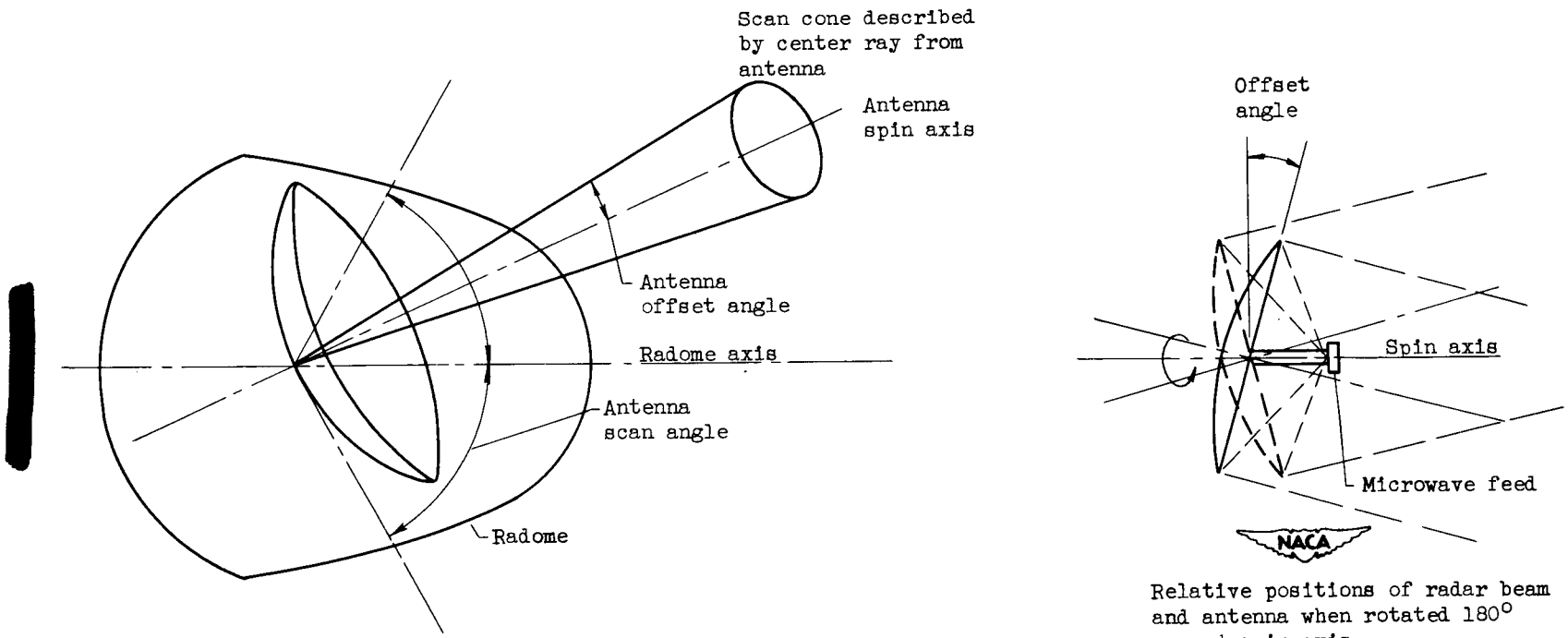

Figure 2. - Sketch showing geometry of conical-scan radar operation.

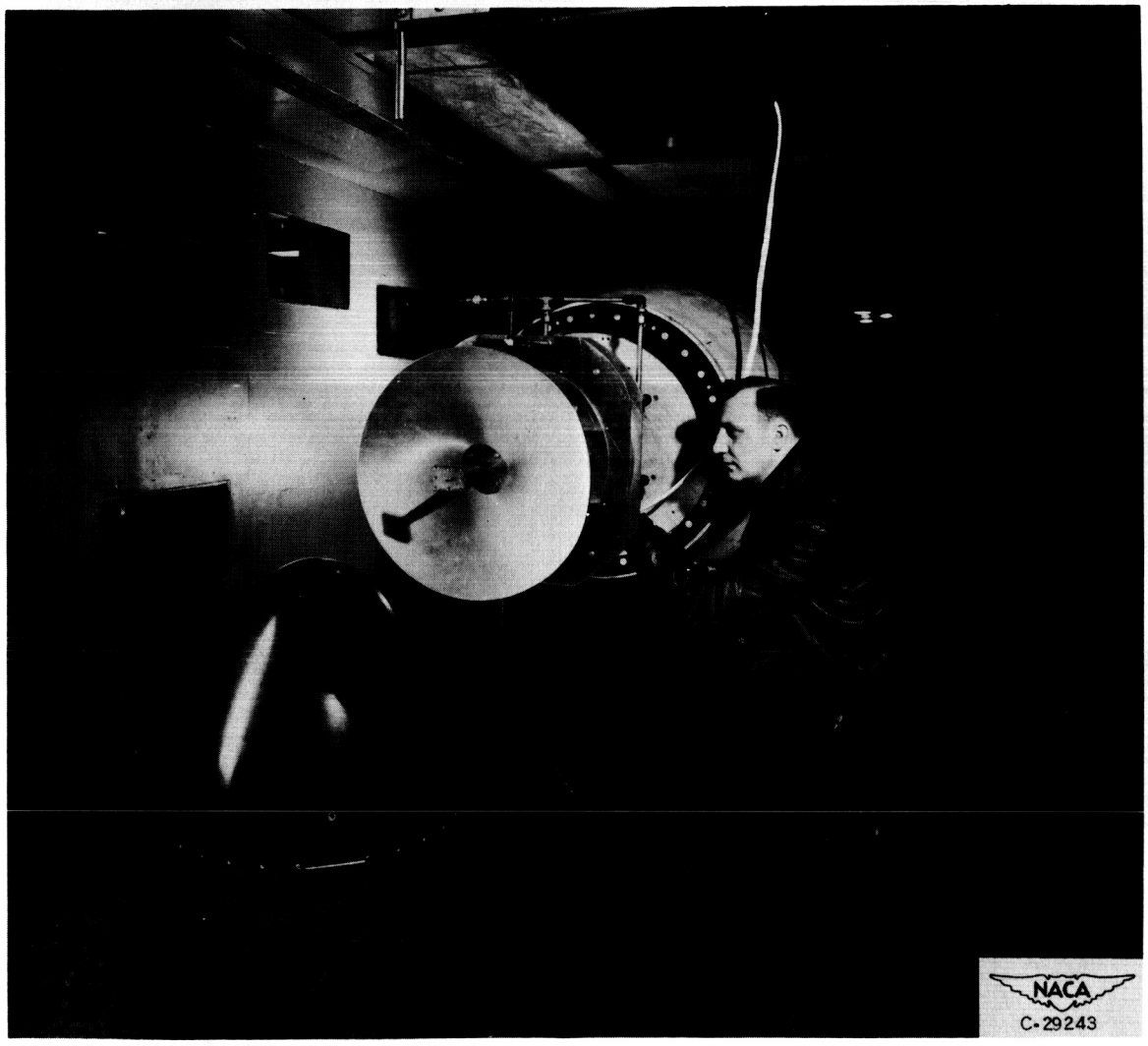

Figure 3. - Test installation with C-radome removed.

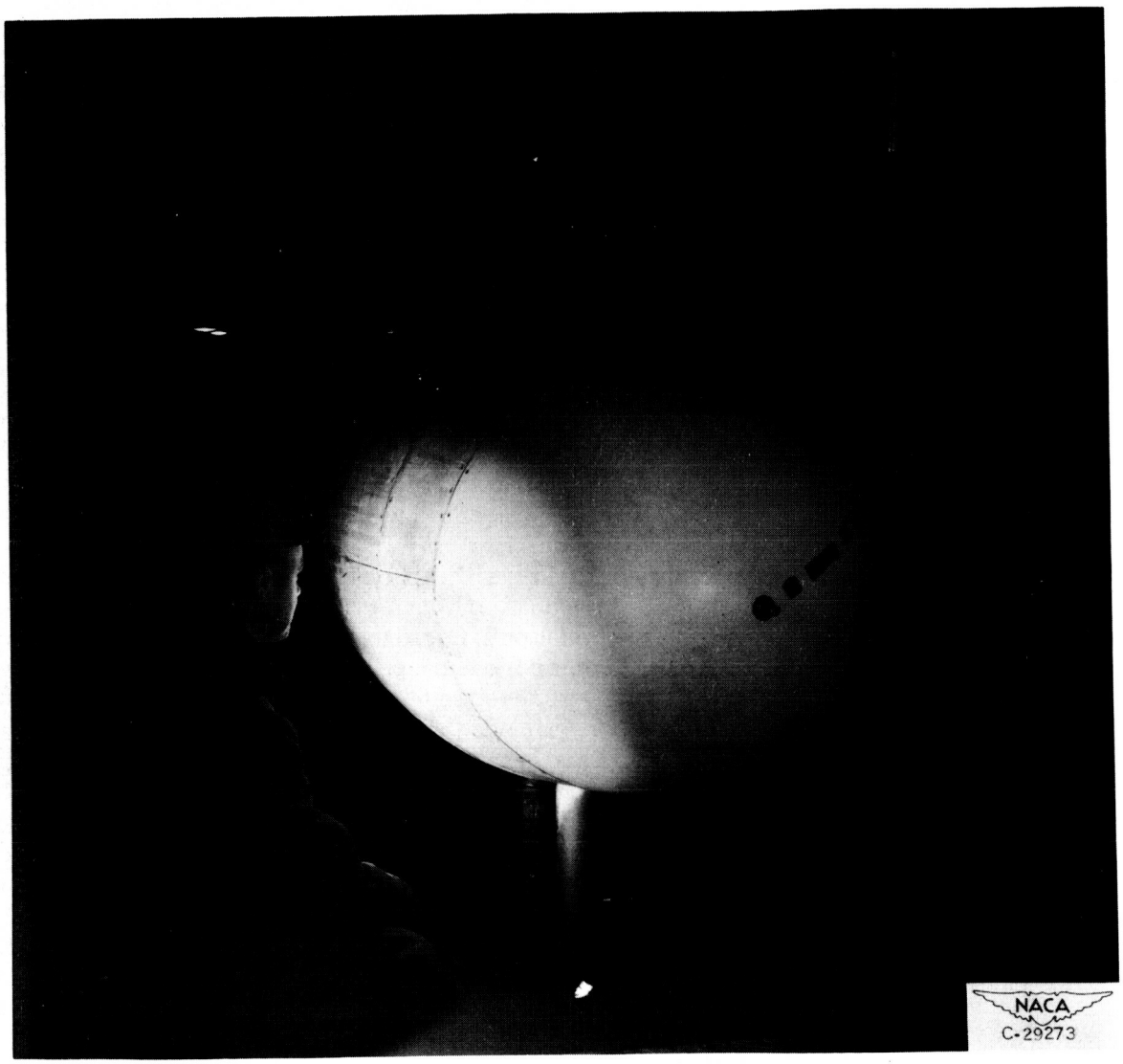

Figure 4. - Installation of test assembly with D-radome in icing tunnel.

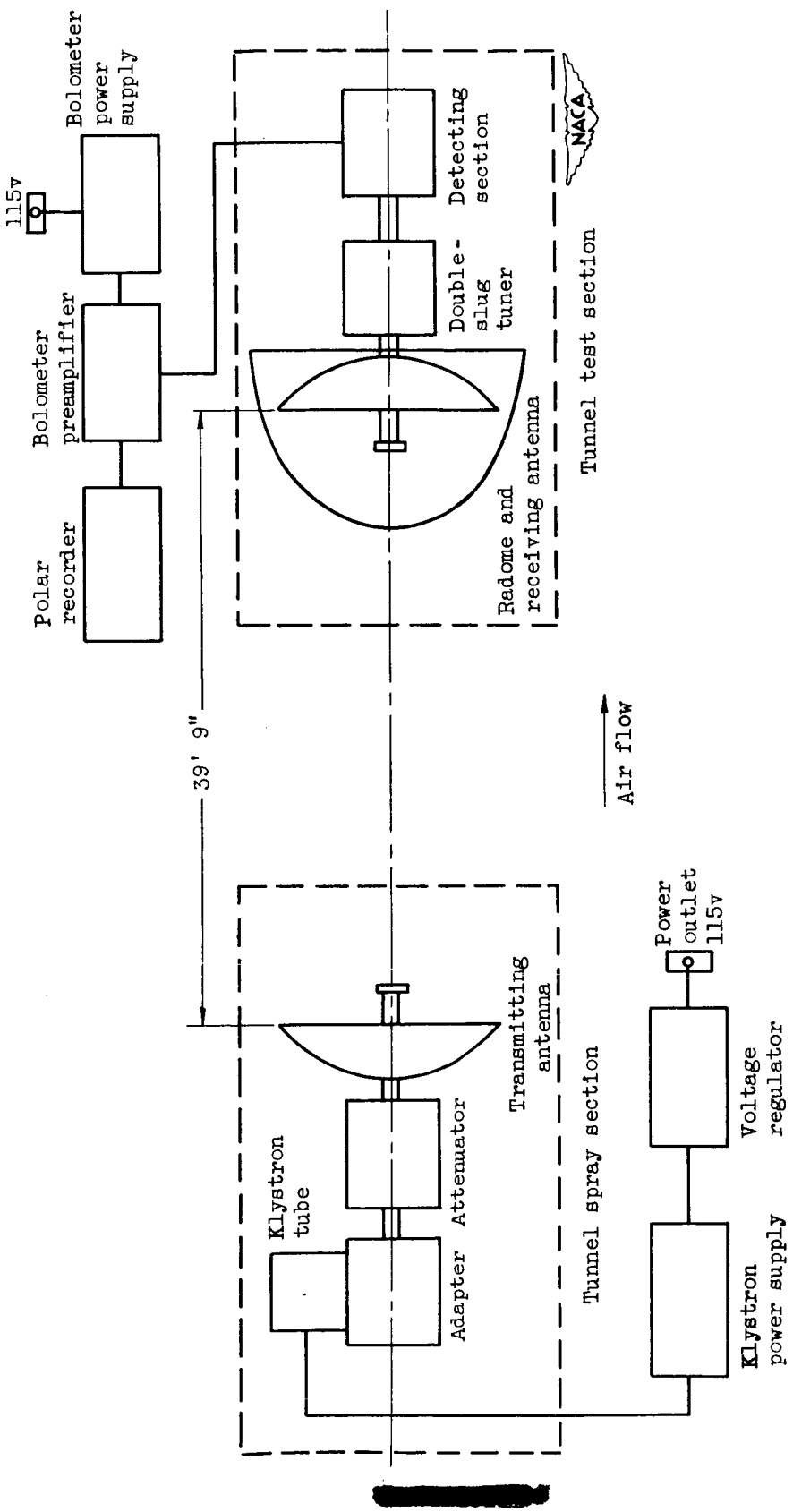

Figure 5. - Sketch of experimental setup for transmission tests.

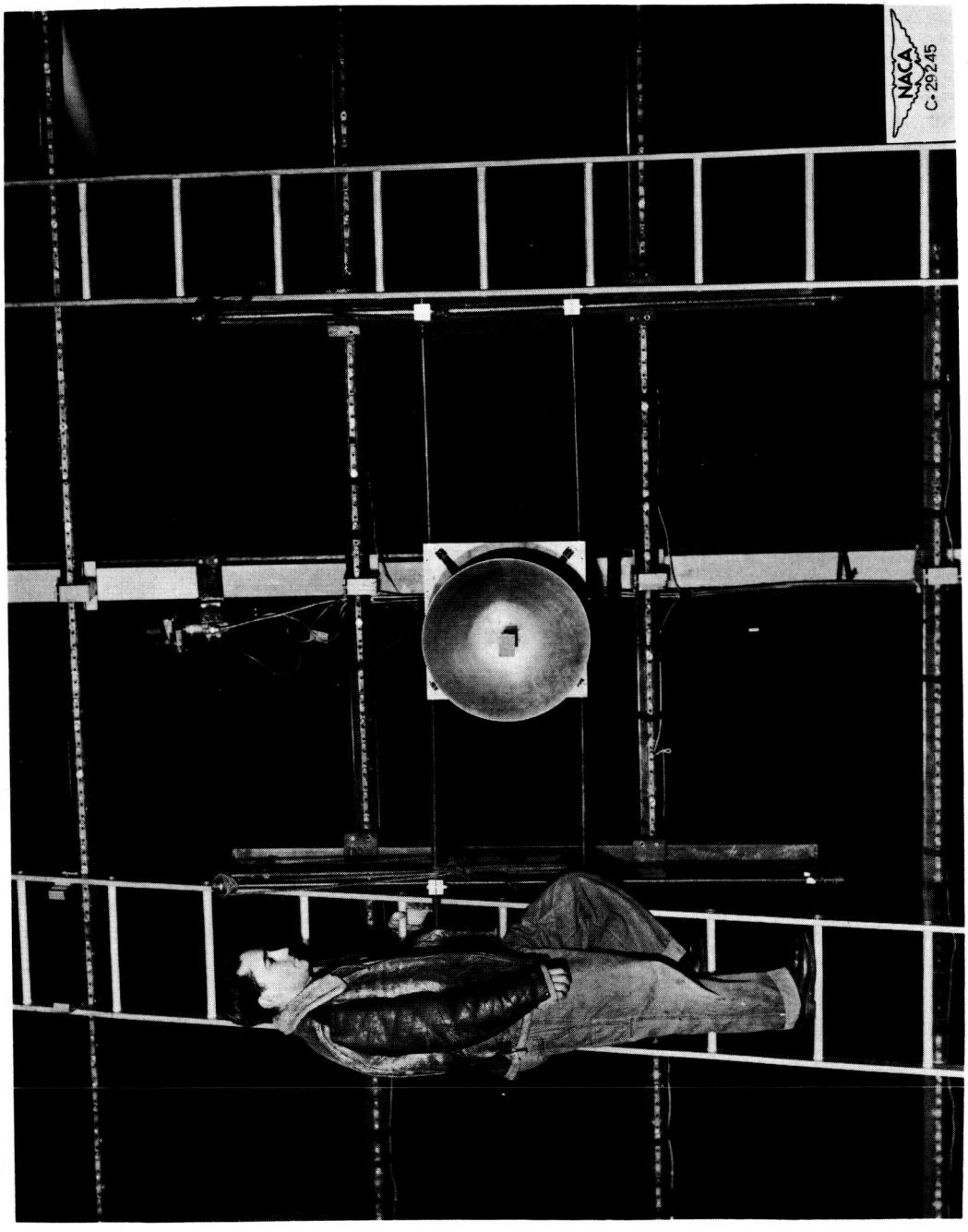

Figure 6. - View of radar antenna mounted on cloud-spray frame.

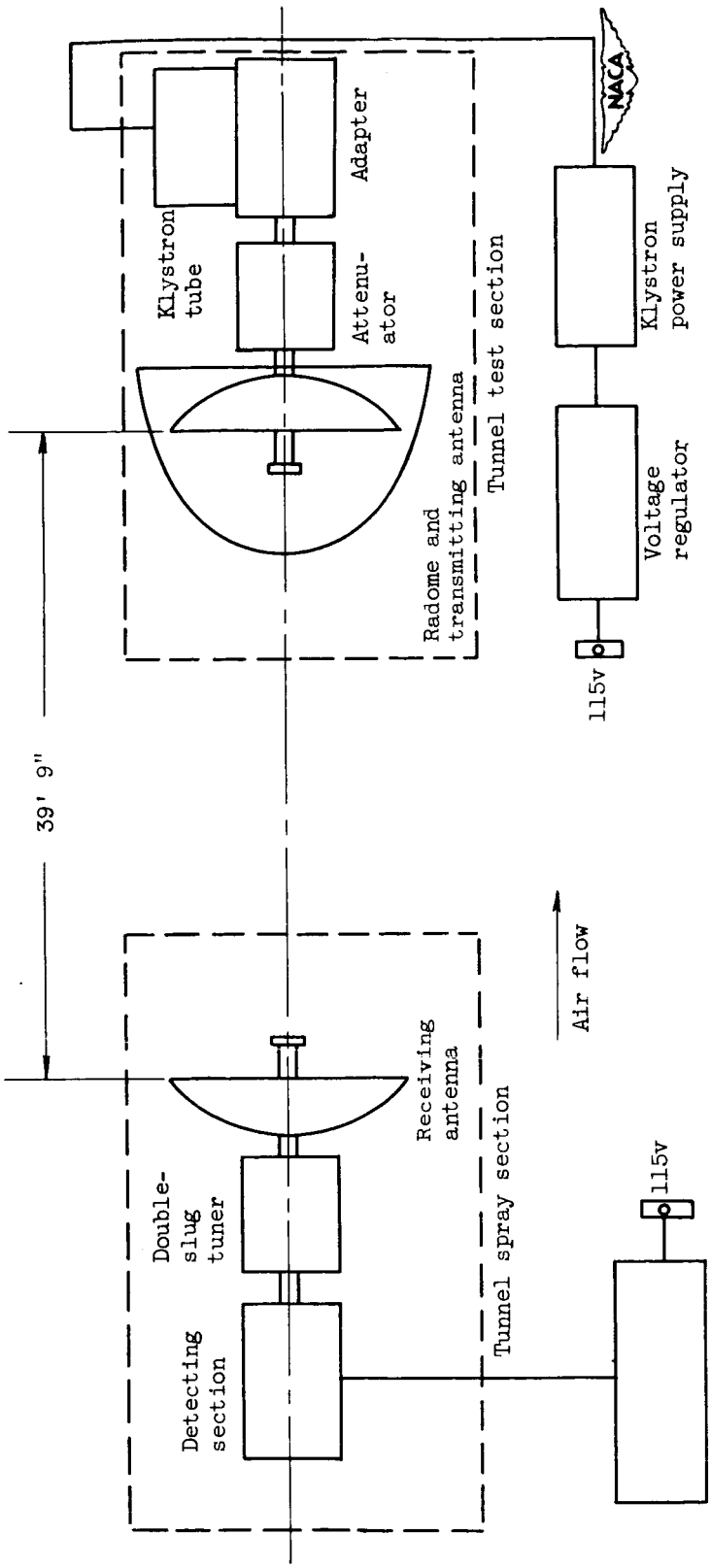

Figure 7. - Sketch of experimental setup for beam-deflection tests.

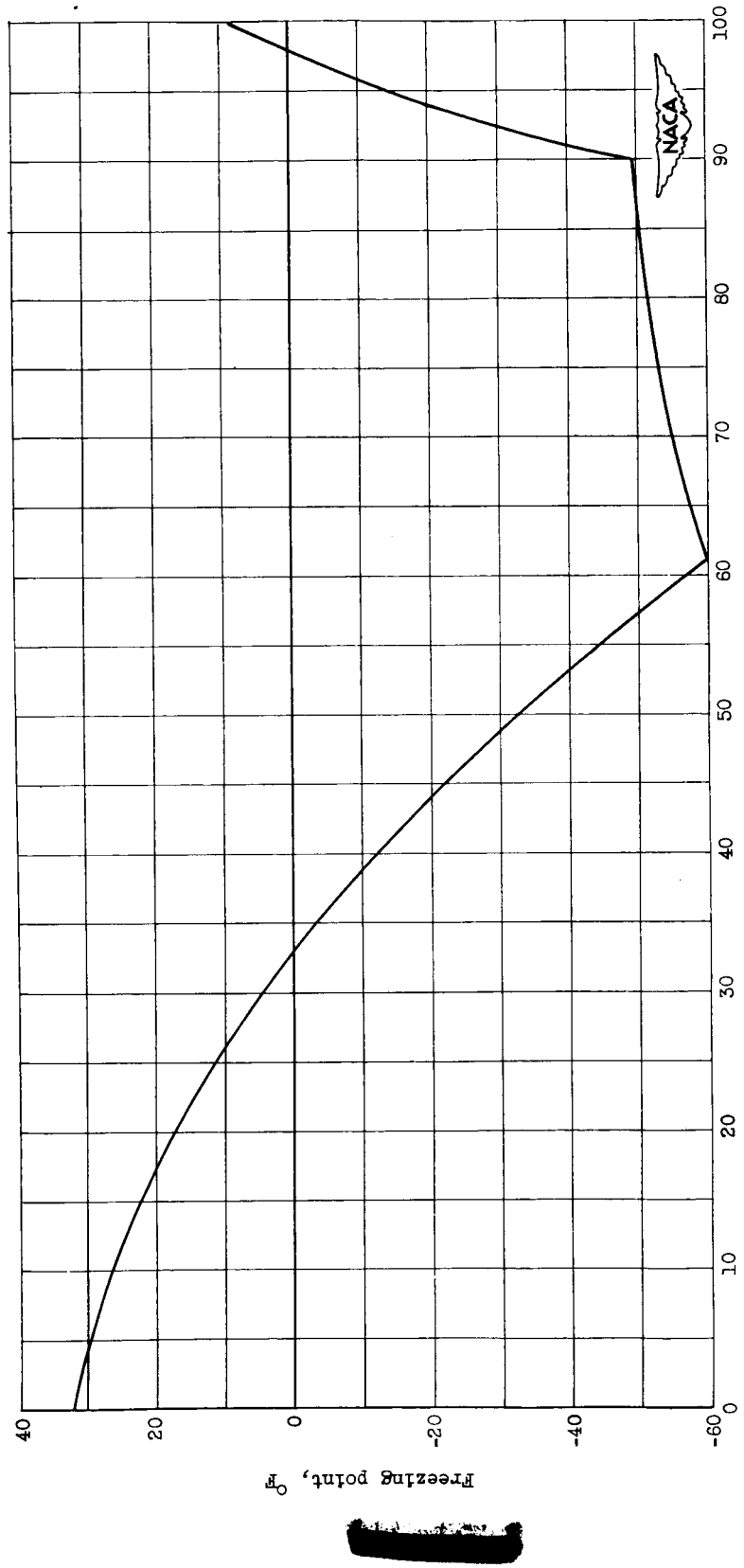

Figure 8. - Freezing point of ethylene glycol - water mixtures.

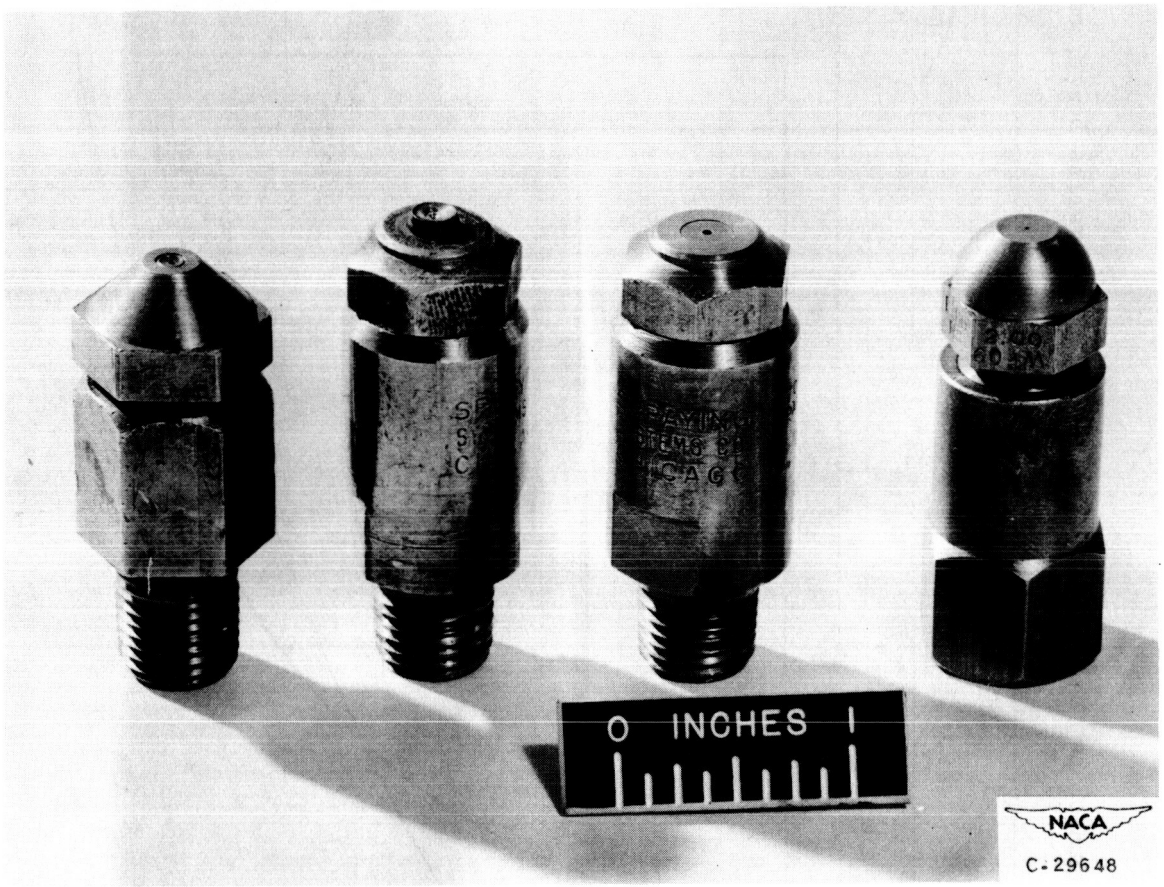

Sprayco J318D | $\frac{1}{4}$ LNN4W | $\frac{1}{4}$ LNN4 | Monarch

Figure 9. - Various fluid-atomizing nozzles.

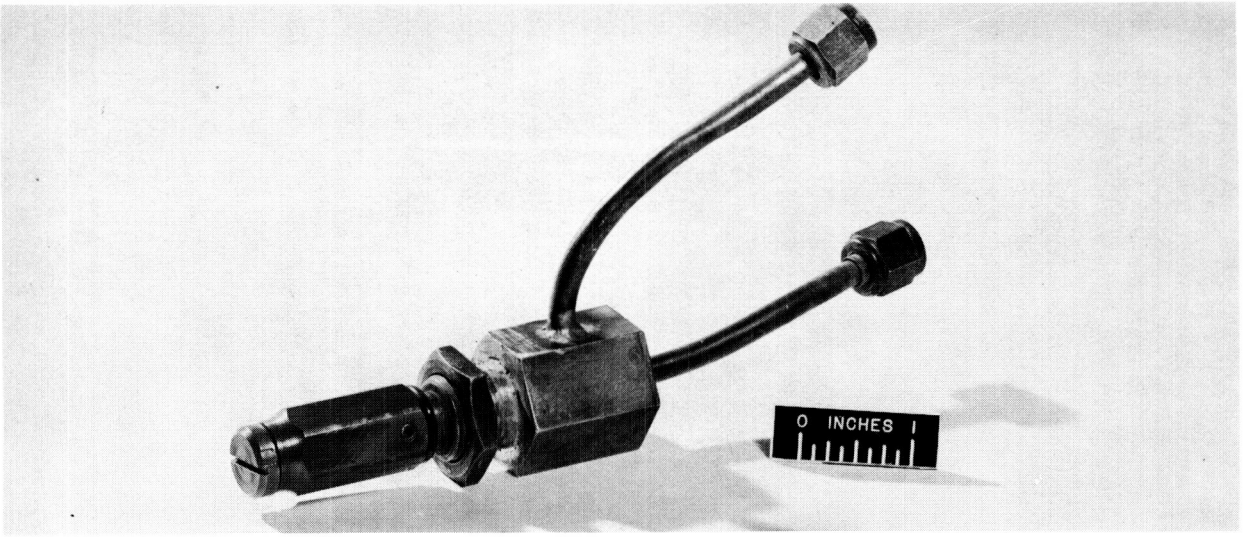

(a) Deflecting type T364M.

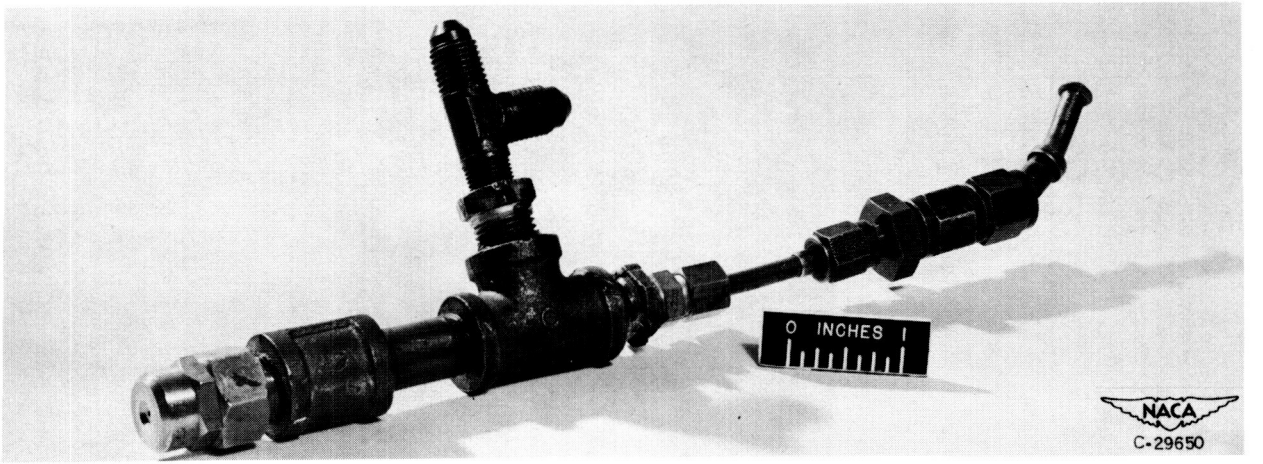

(b) Nondeflecting type.

Figure 10. - Air-atomizing nozzles used in icing-protection system.

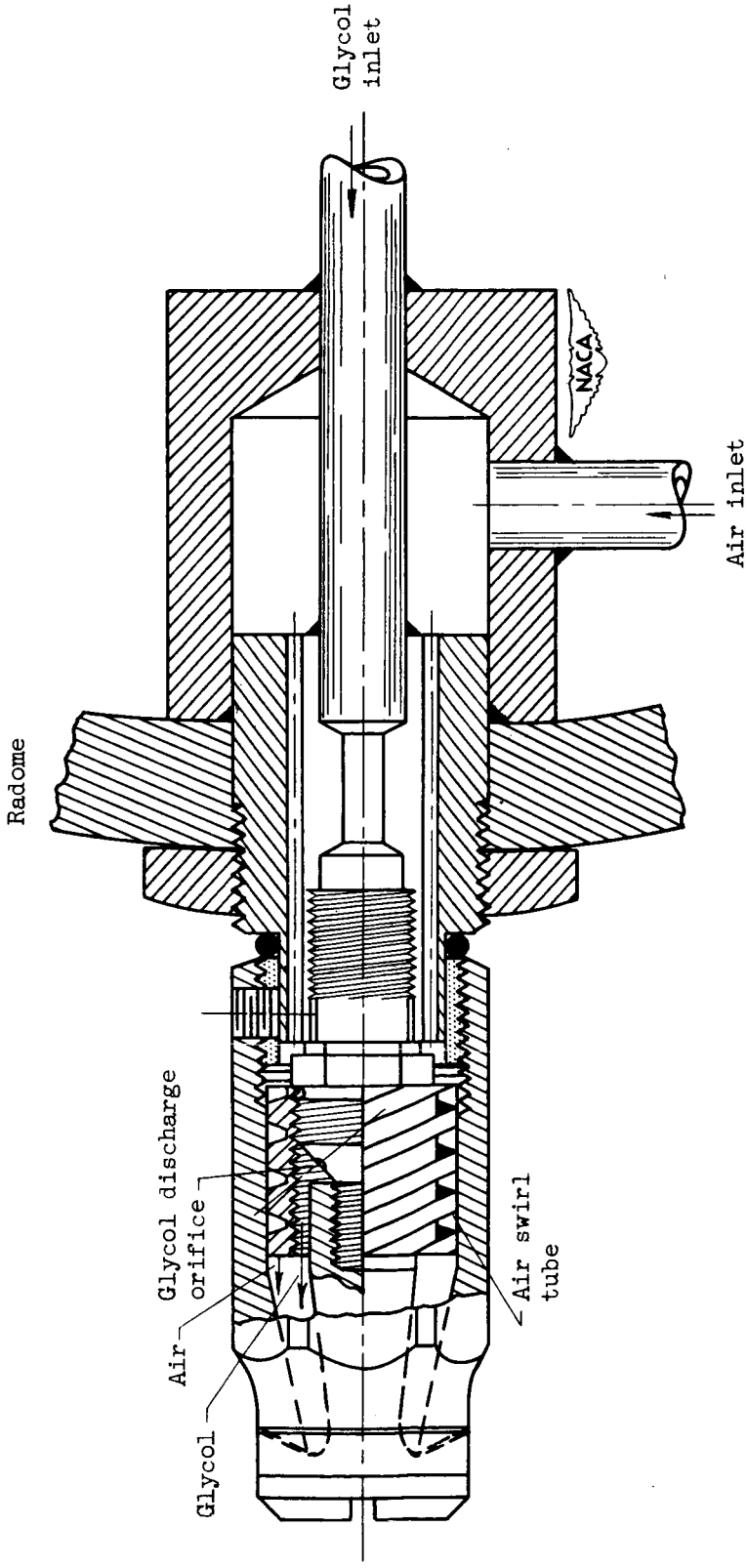

Figure 11. - Sketch of T364M nozzle installation.

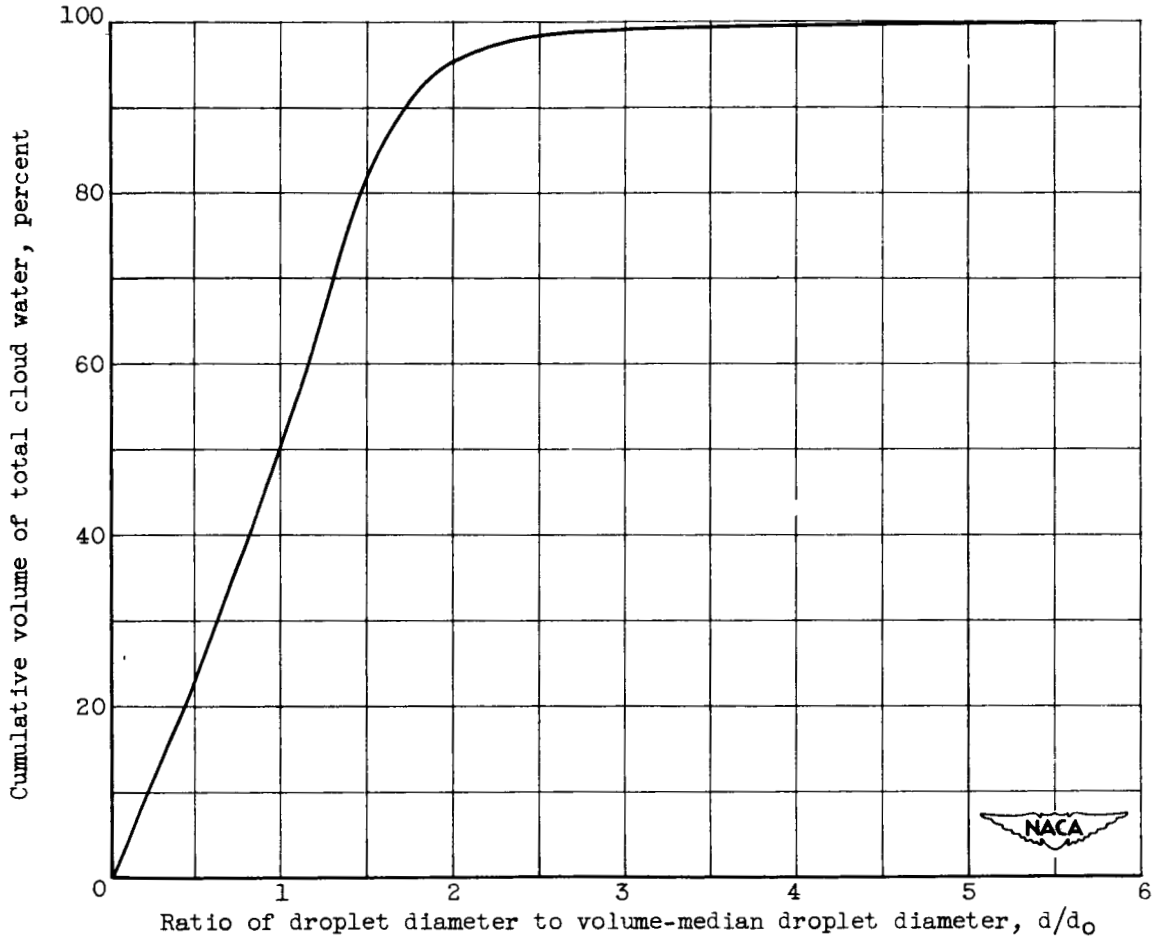

Figure 12. - Droplet-size distribution in icing research tunnel for radome water-impingement investigation.

2681

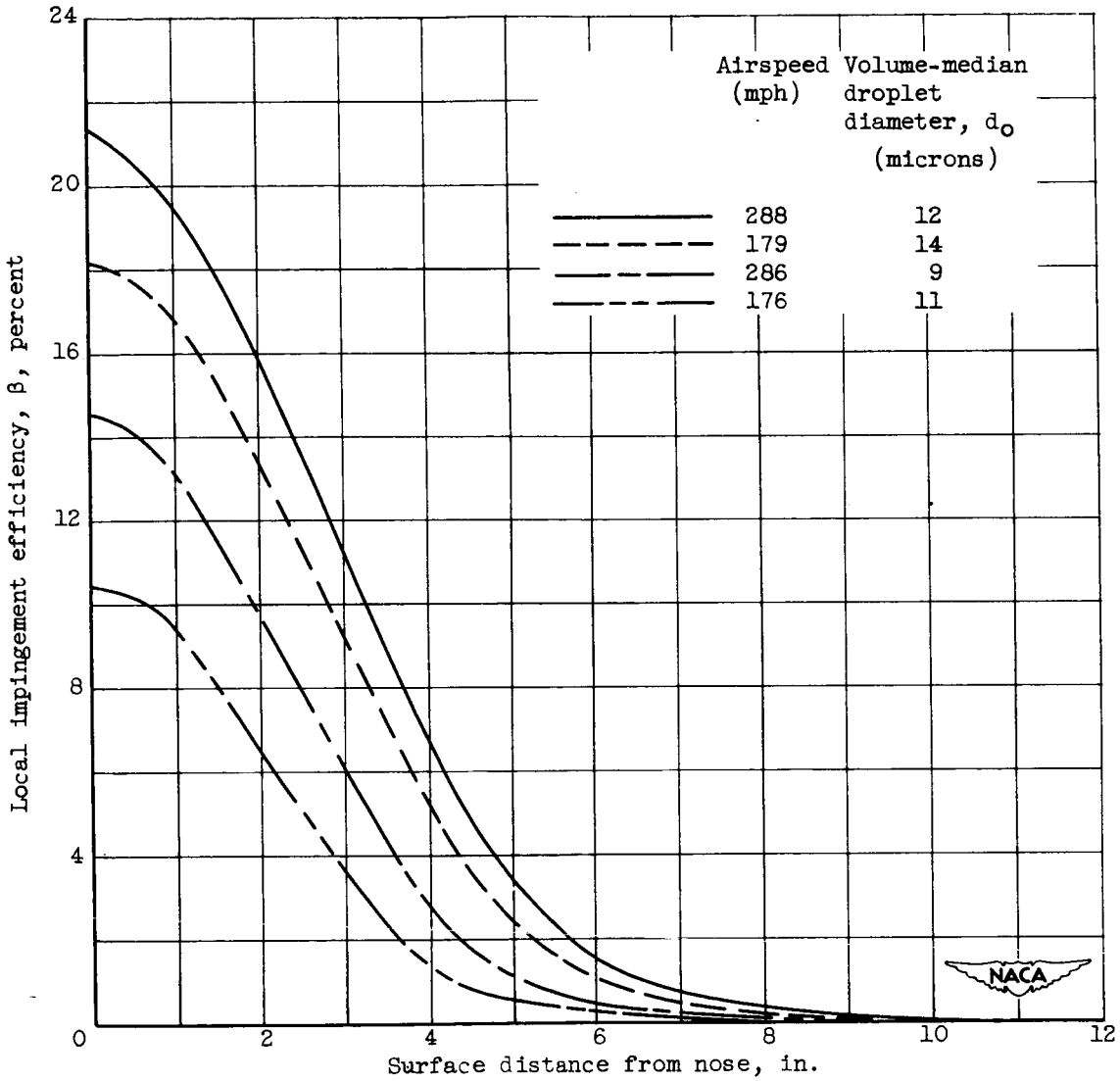

(a) Angle of attack, 0°.

Figure 13. - Distribution of water-droplet impingement on C-radome.

[redacted]

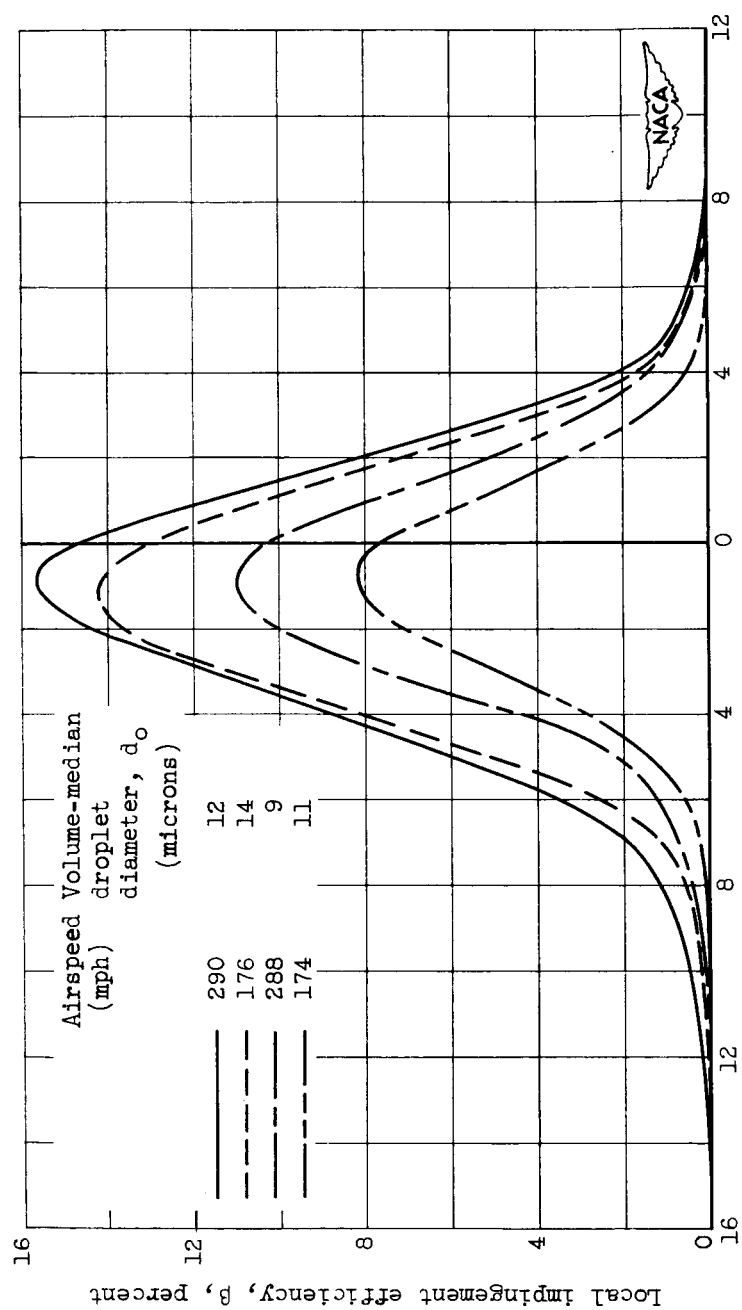

(b) Angle of attack, 4°.

Figure 13. - Concluded. Distribution of water-droplet impingement on C-radome.

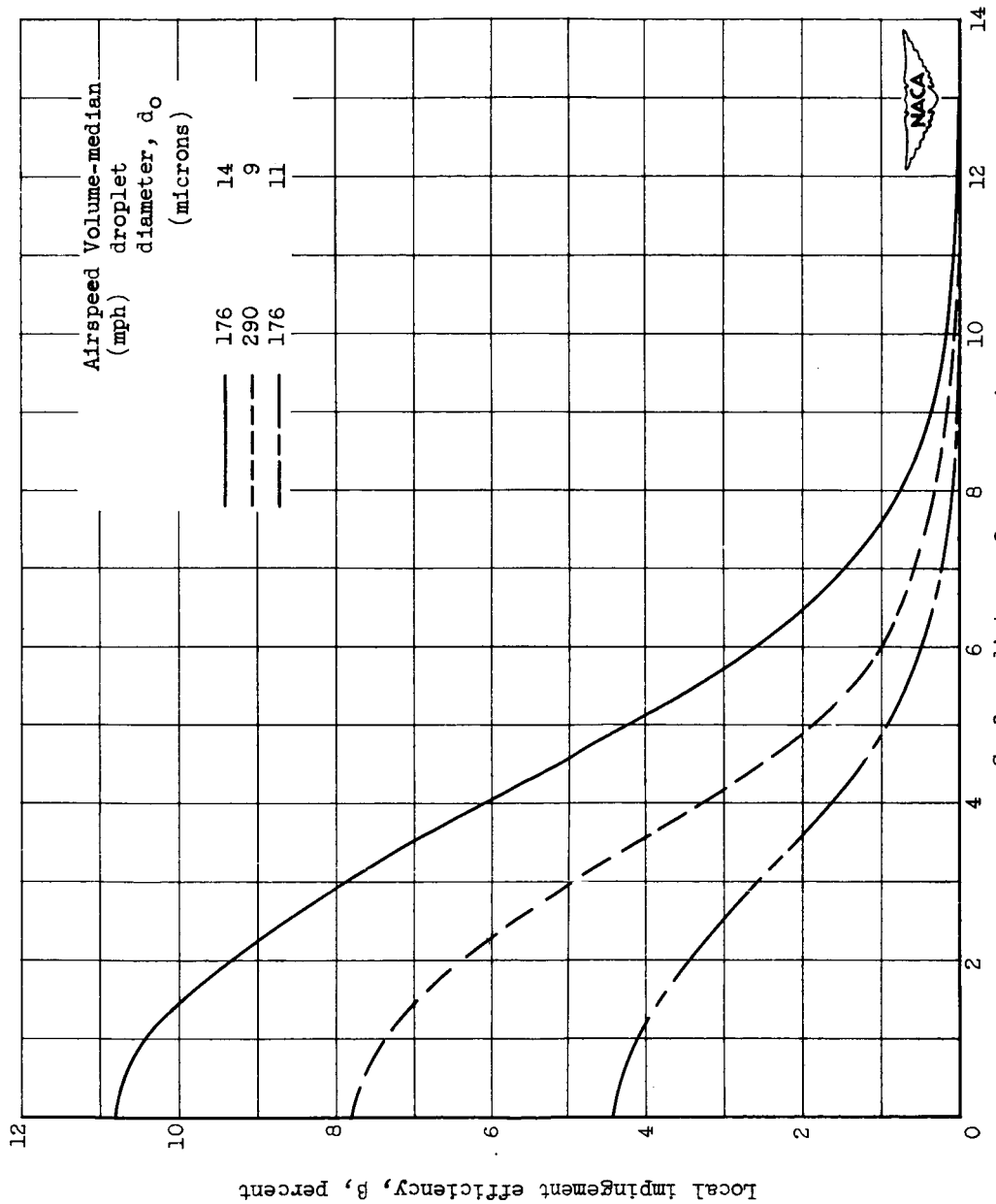

(a) Angle of attack, 0°.

Figure 14. - Distribution of water-droplet impingement on D-radome.

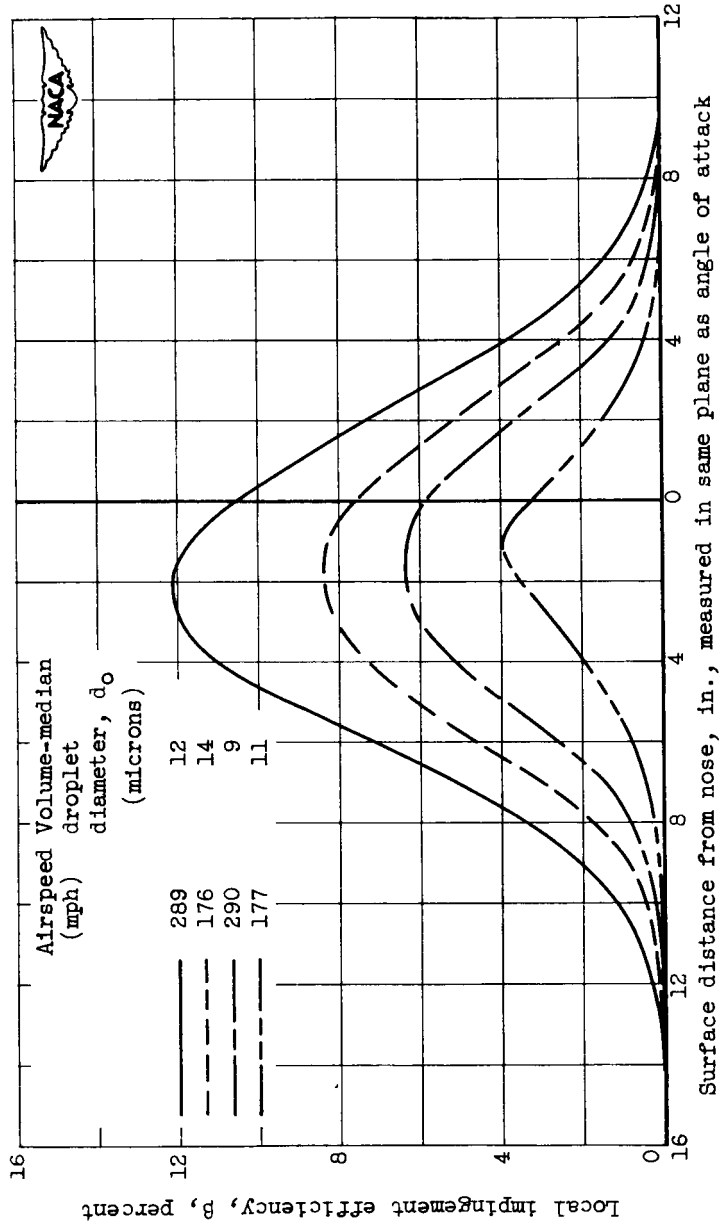

(b) Angle of attack, 4°.

Figure 14. - Concluded. Distribution of water-droplet impingement on D-radome.

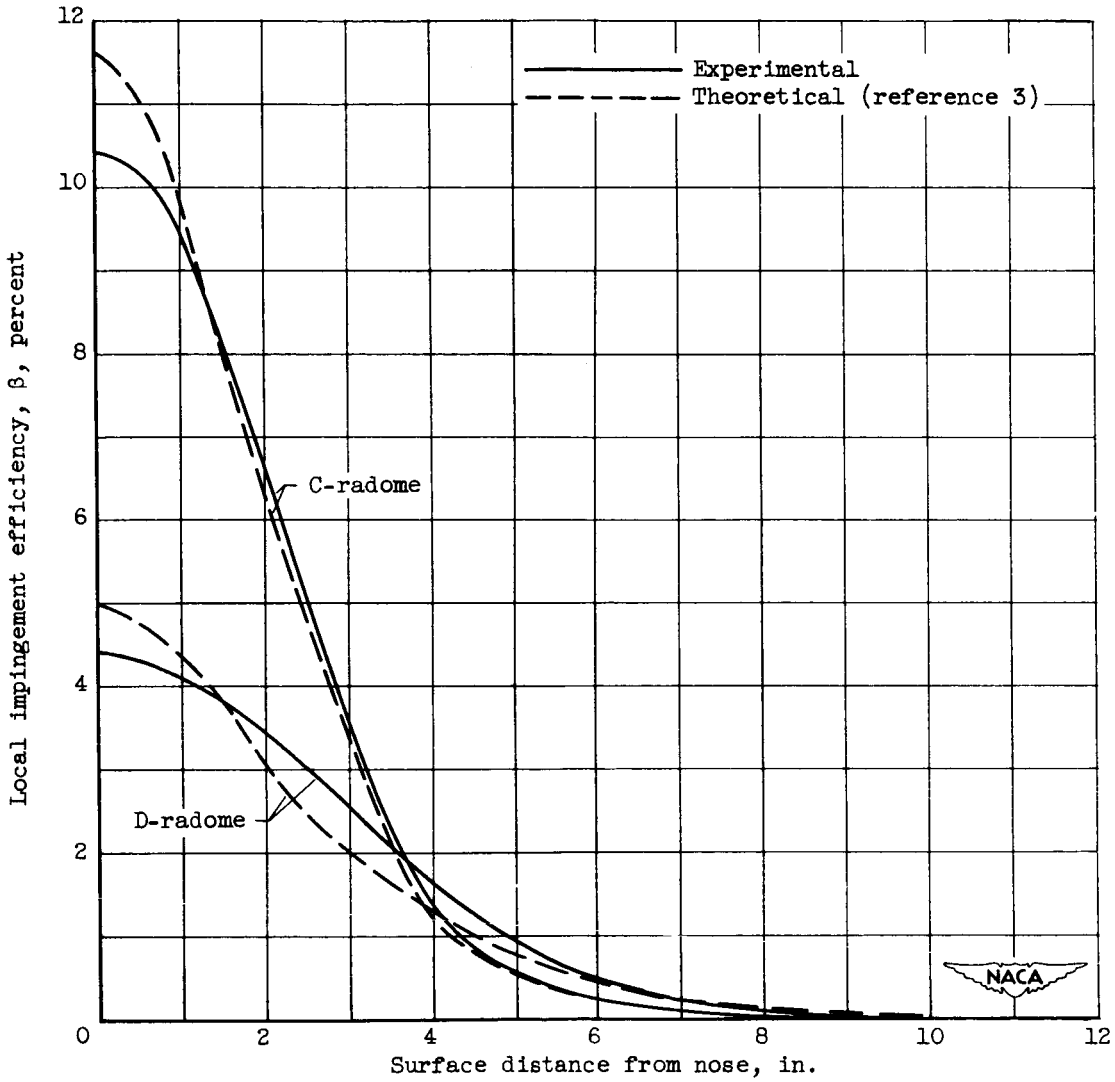

Figure 15. - Comparison of impingement on radomes and theoretical sphere values. Airspeed, 176 miles per hour; volume-median droplet size, 11 microns; angle of attack, 0°. Droplet-size distribution is that of figure 12.

[redacted]

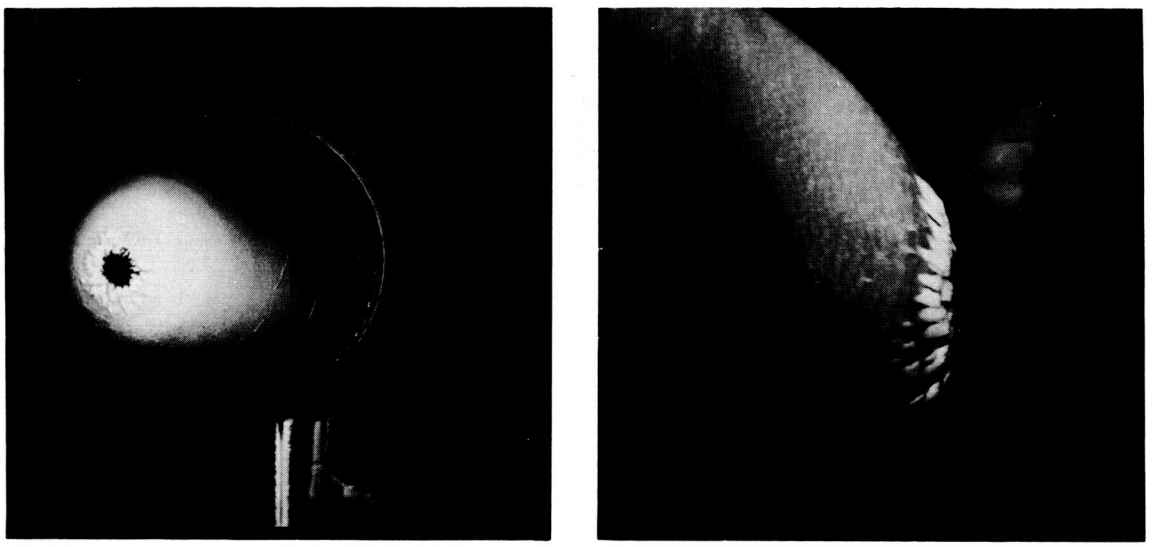

(a) Velocity, 168 miles per hour; angle of attack, 0°; tunnel total temperature, 10° F; liquid-water content, 0.8 gram per cubic meter.

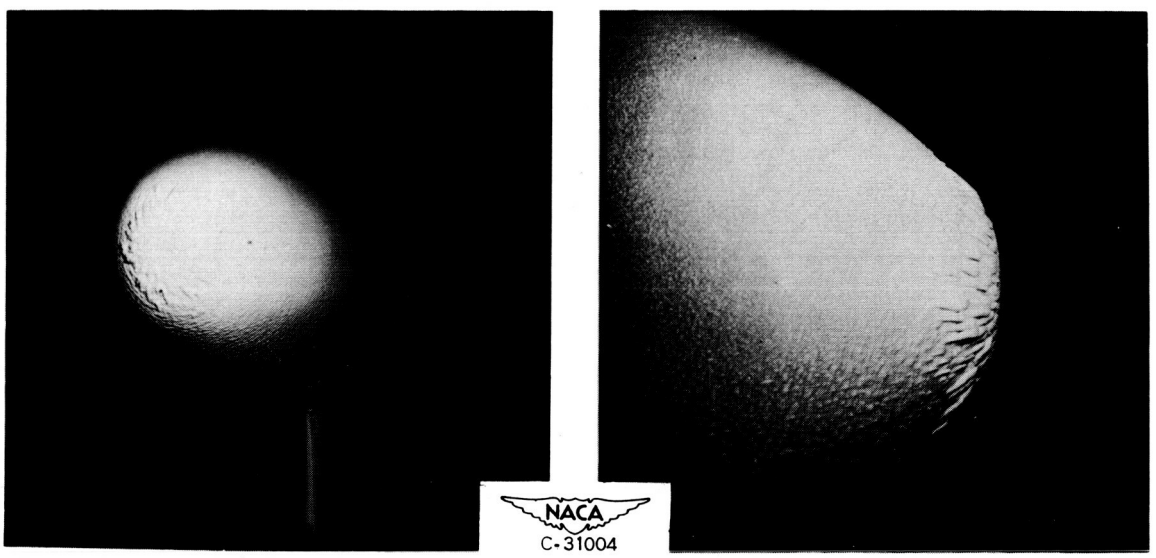

(b) Velocity, 273 miles per hour; angle of attack, 0°; tunnel total temperature, -5° F; liquid-water content, 0.85 gram per cubic meter.

Figure 16. - Views of C-radome after 15 minutes icing.

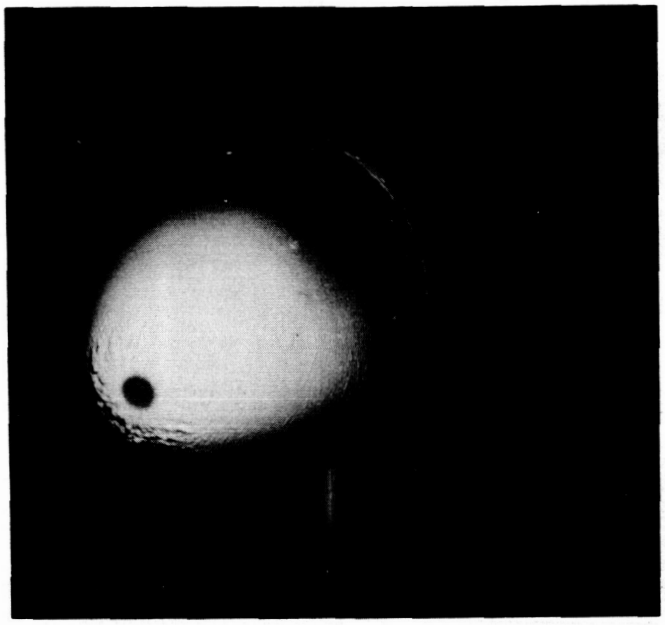

(c) Velocity, 276 miles per hour; angle of attack, 0° ; tunnel total temperature, 5° F; liquid-water content, 0.95 gram per cubic meter.

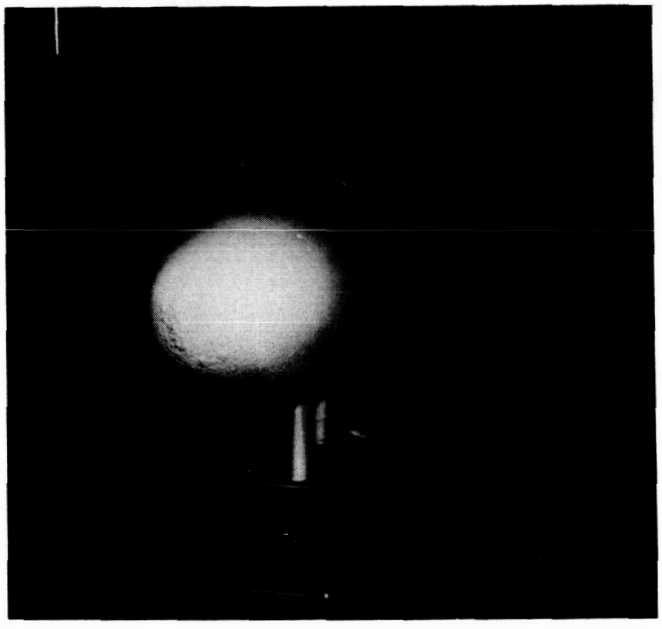

(d) Velocity, 278 miles per hour; angle of attack, 4° ; tunnel total temperature, -6° F; liquid-water content, 0.85 gram per cubic meter.

Figure 16. - Concluded. Views of C-radome after 15 minutes icing.

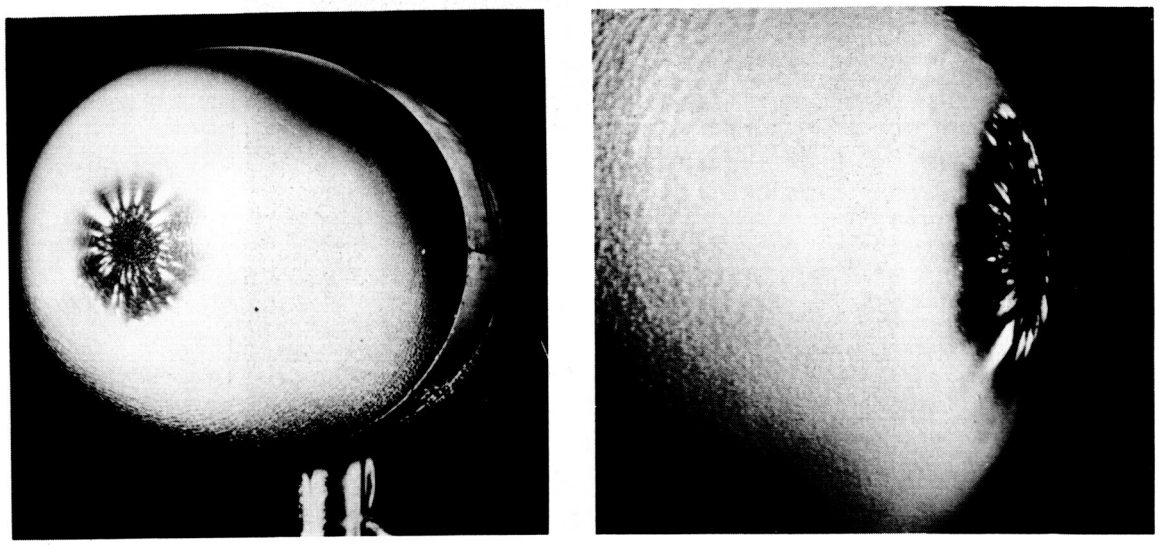

(a) Velocity, 168 miles per hour; angle of attack, 0°; tunnel total temperature, 9° F; liquid-water content, 0.8 gram per cubic meter.

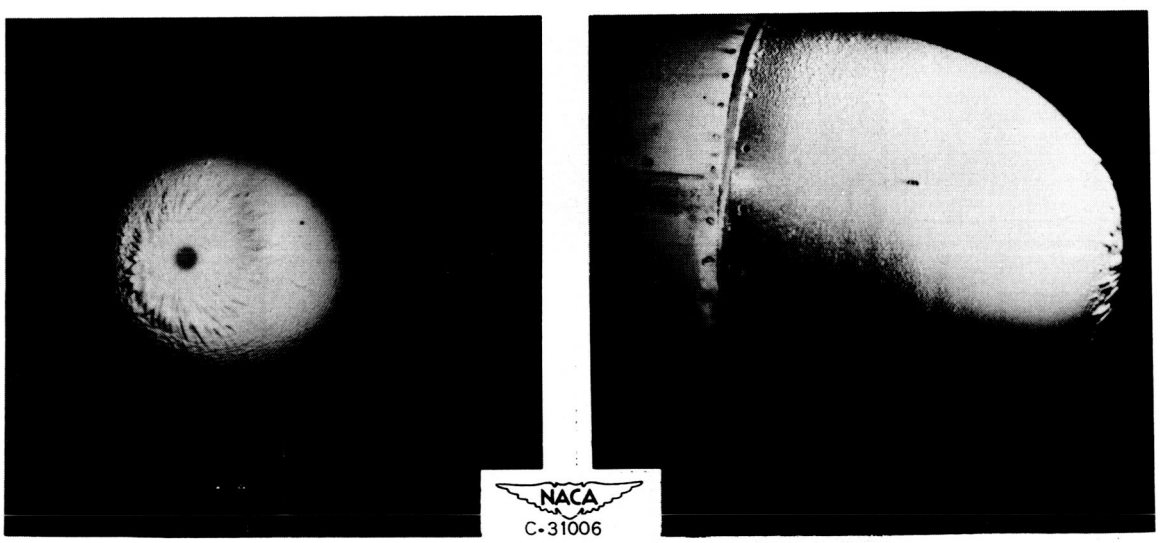

(b) Velocity, 275 miles per hour; angle of attack, 0°; tunnel total temperature, -4° F; liquid-water content, 0.85 gram per cubic meter.

Figure 17. - Views of D-radome after 15 minutes icing.

[redacted]

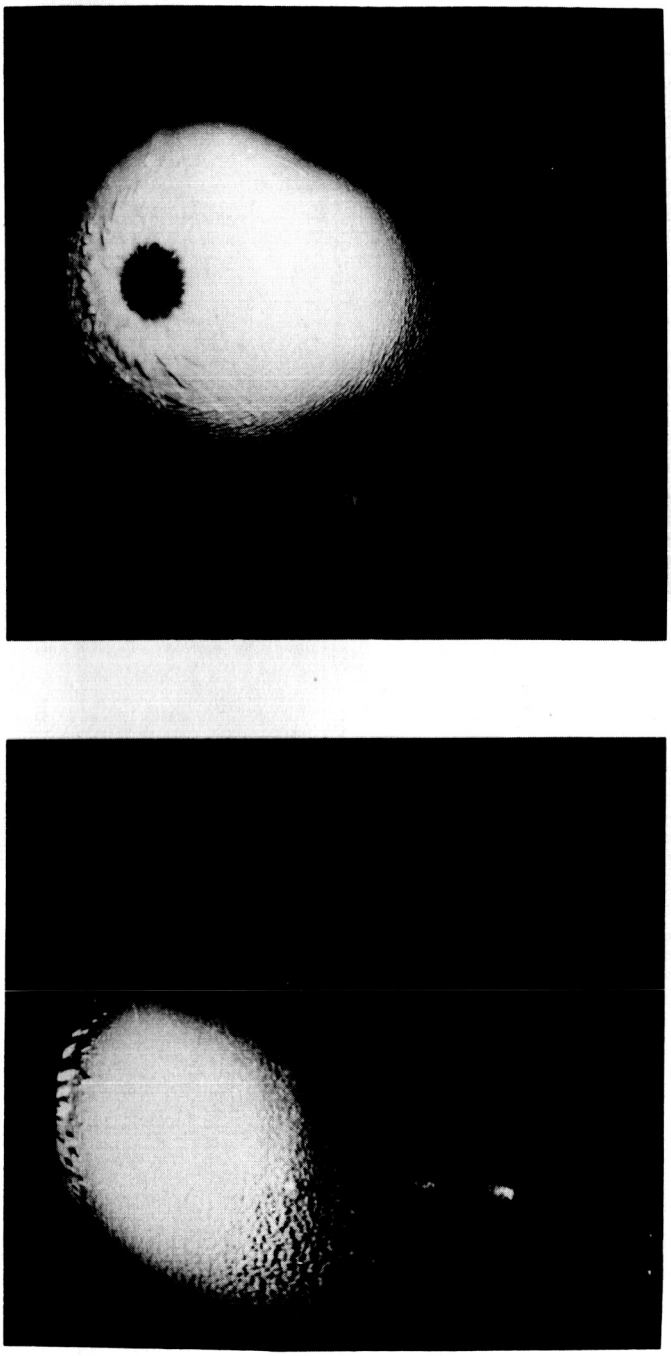

(c) Velocity, 274 miles per hour; angle of attack, 0°; tunnel total temperature, 12° F; liquid-water content, 0.9 gram per cubic meter.

Figure 17. - Concluded. Views of D-radome after 15 minutes icing.

[redacted]

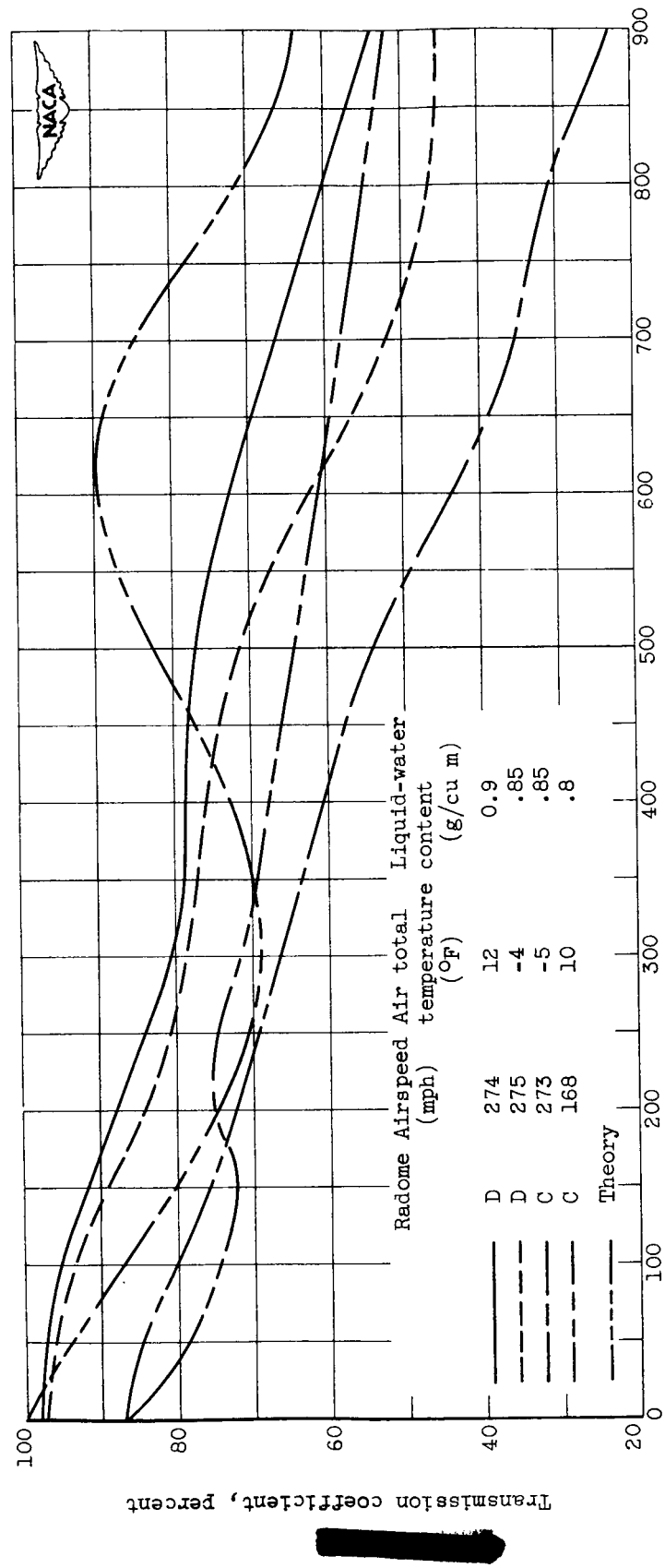

Figure 18. - Transmission through cloud and radome during icing period.

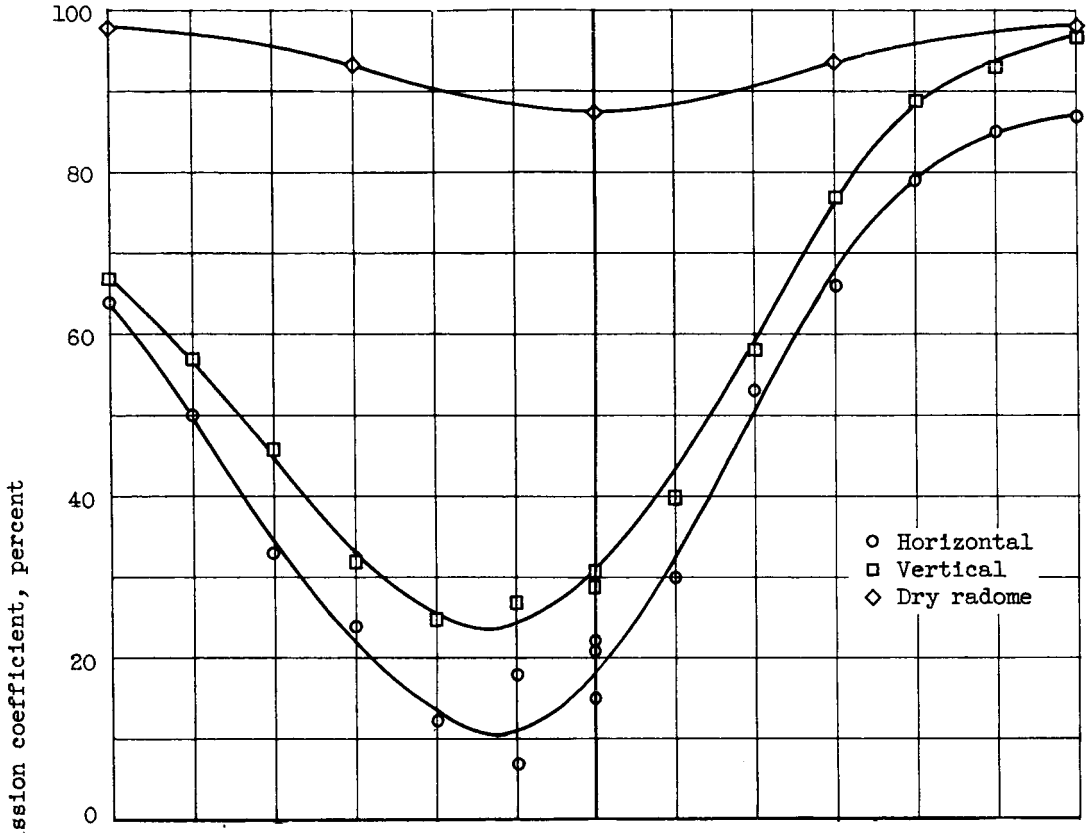

(a) Airspeed, 273 miles per hour; air total temperature, -5° F; liquid-water content, 0.85 gram per cubic meter.

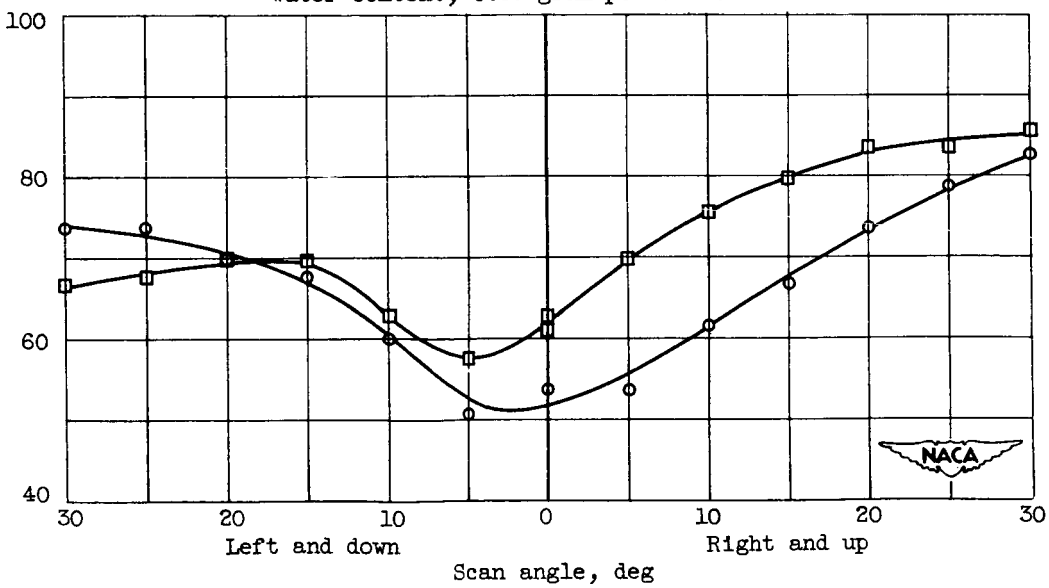

(b) Airspeed, 168 miles per hour; air total temperature, 10° F; liquid-water content, 0.8 gram per cubic meter.

Figure 19. - Transmission through C-radome after 15 minutes icing at zero angle of attack.

[redacted]

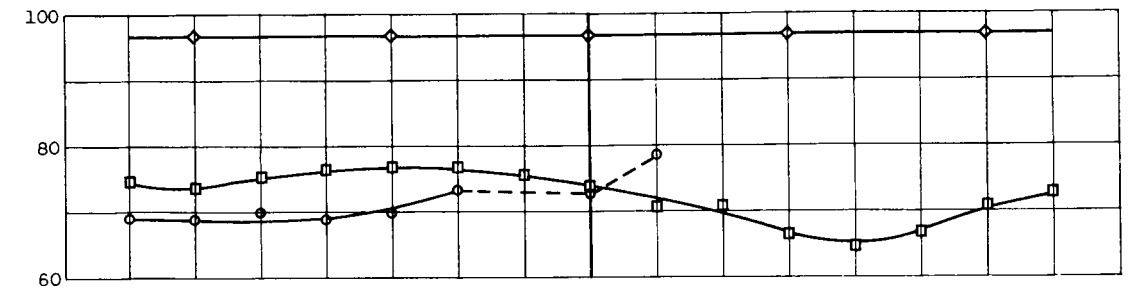

(a) Airspeed, 168 miles per hour; air total temperature, 9° F; liquid-water content, 0.8 gram per cubic meter.

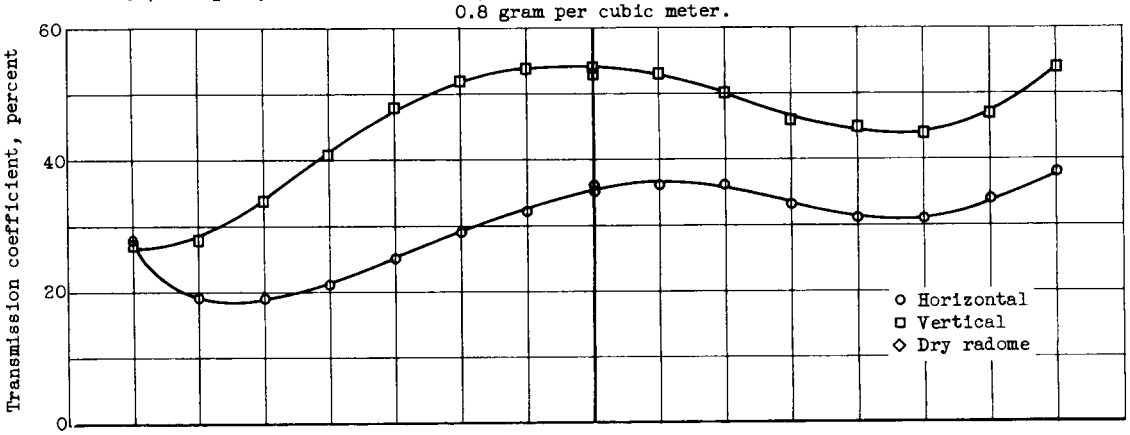

(b) Airspeed, 275 miles per hour; air total temperature, -4° F; liquid-water content, 0.85 gram per cubic meter.

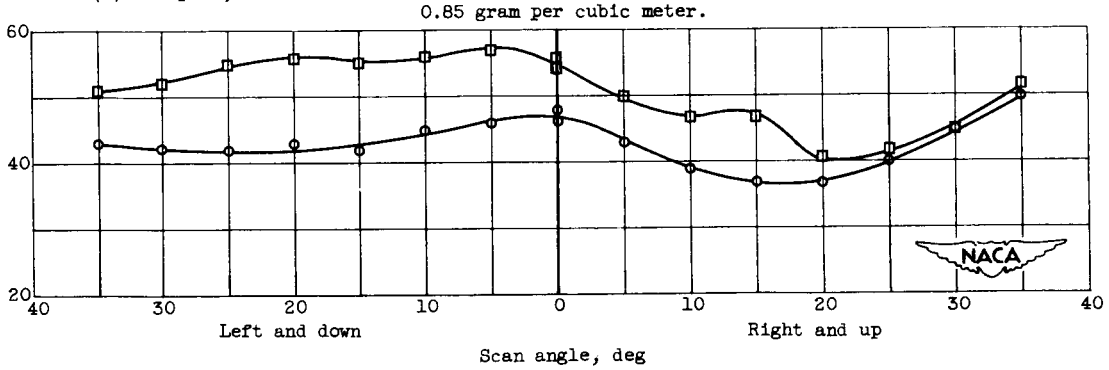

(c) Airspeed, 274 miles per hour; air total temperature, 12° F; liquid-water content, 0.9 gram per cubic meter.

Figure 20. - Transmission through D-radome after 15 minutes icing at zero angle of attack.

[redacted]

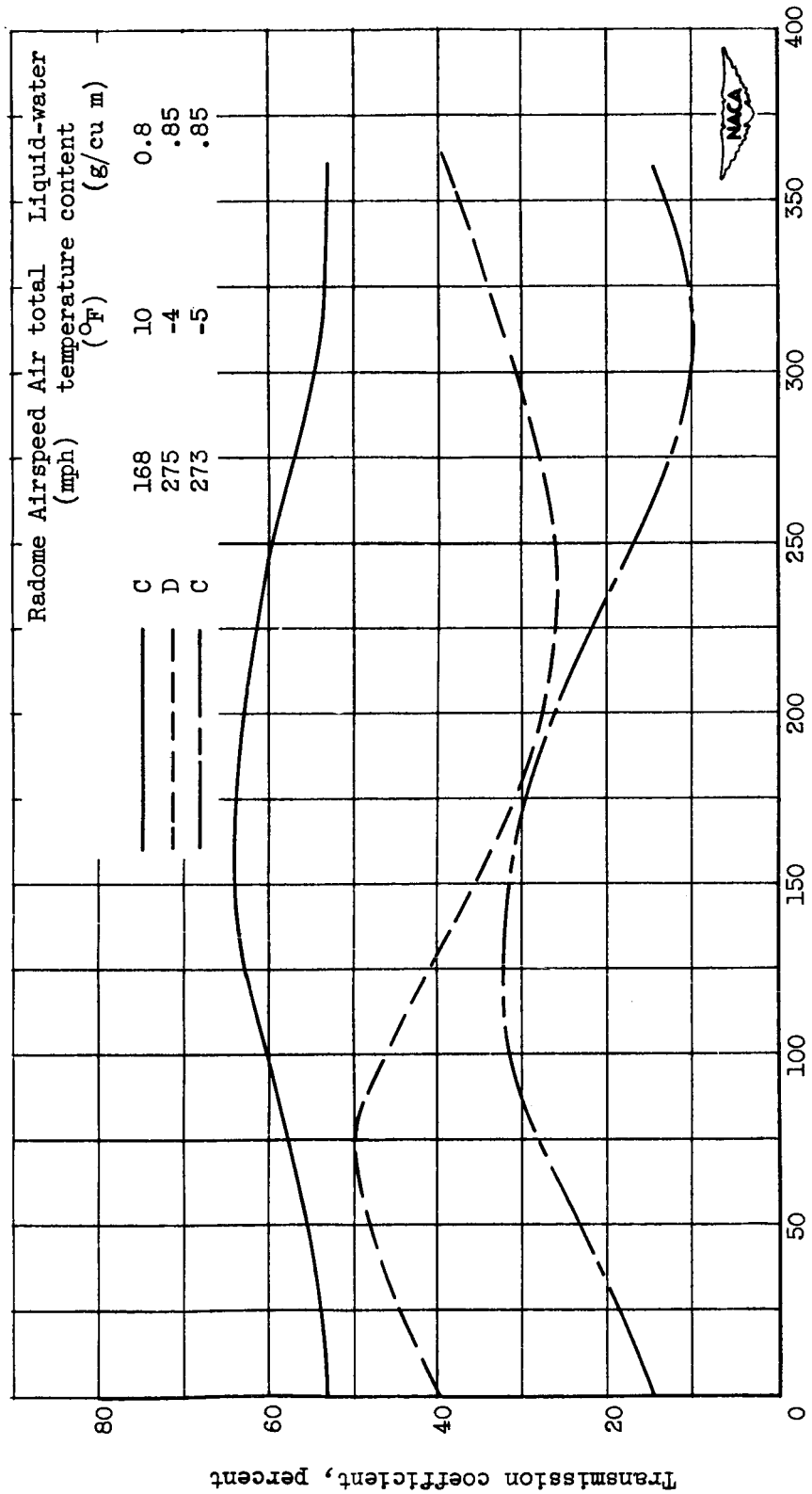

Figure 21. - Transmission through rotating radomes after 15 minutes icing at zero angle of attack.

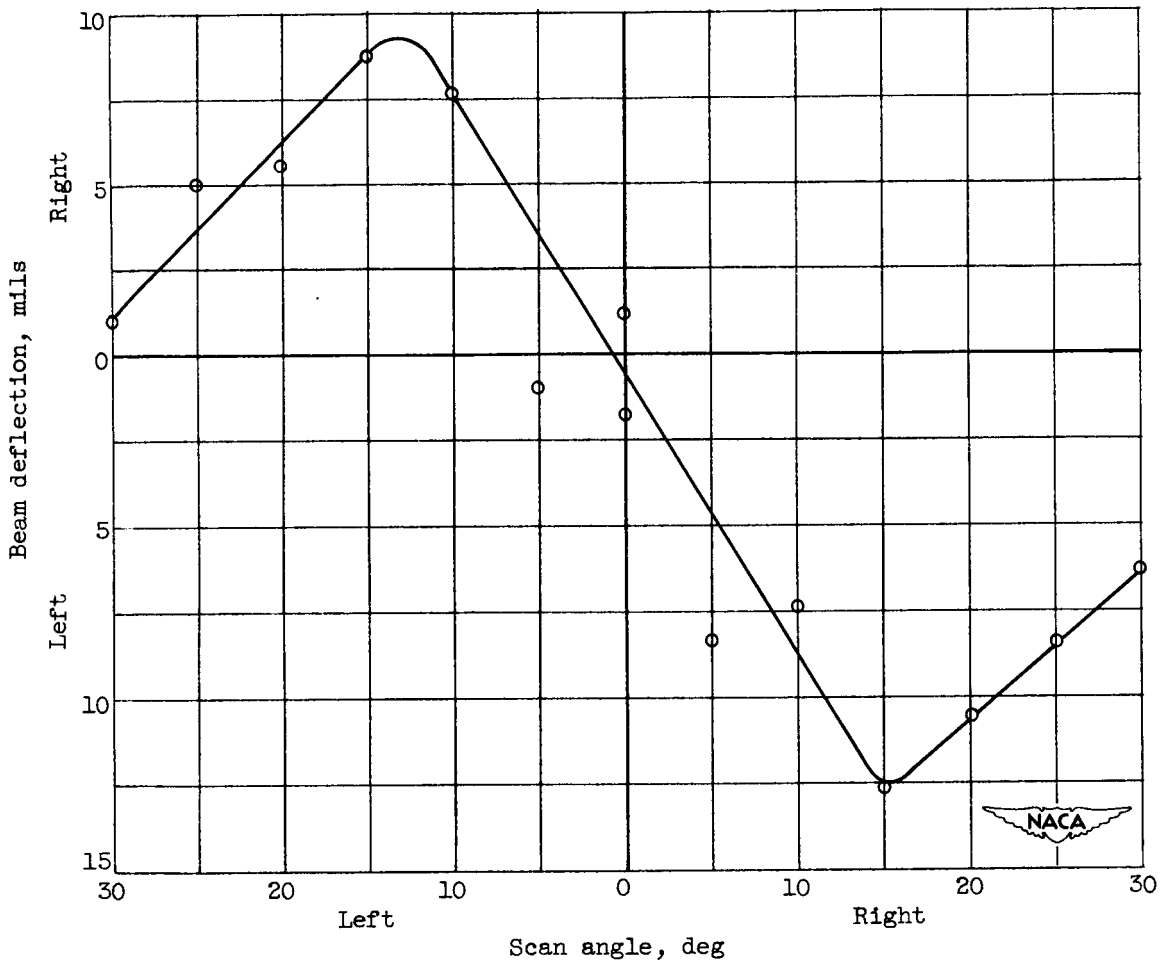

(a) Radome in normal position.

Figure 22. - Component of deflection of radar beam in azimuth plane by iced radome after 15 minutes icing at zero angle of attack. Airspeed, 276 miles per hour; air total temperature, 5° F; liquid-water content, 0.95 gram per cubic meter.

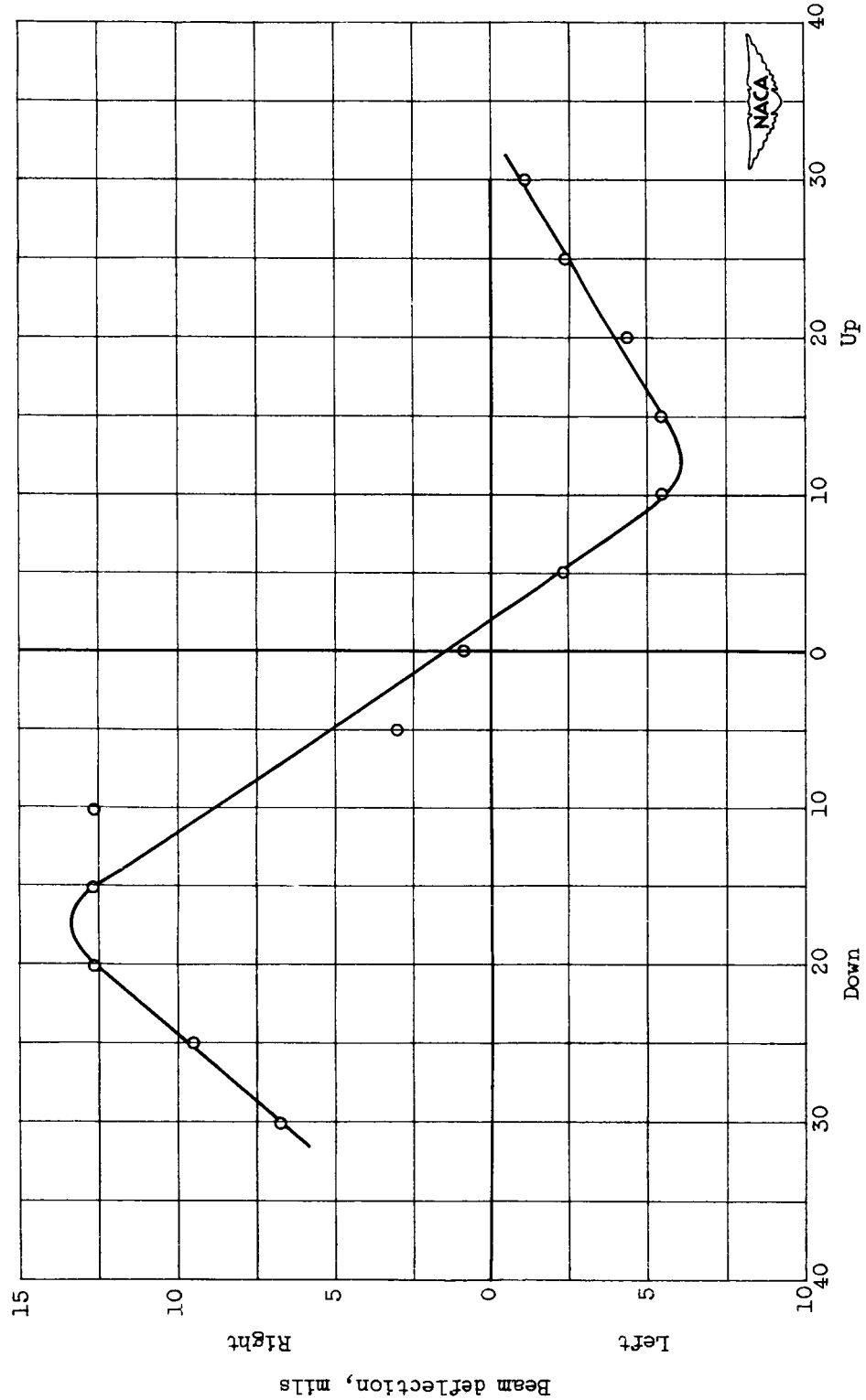

(b) Radome rotated 90°.

Figure 22. - Concluded. Component of deflection of radar beam in azimuth plane by iced radome after 15 minutes icing at zero angle of attack. Airspeed, 276 miles per hour; air total temperature, 5° F; liquid-water content, 0.95 gram per cubic meter.

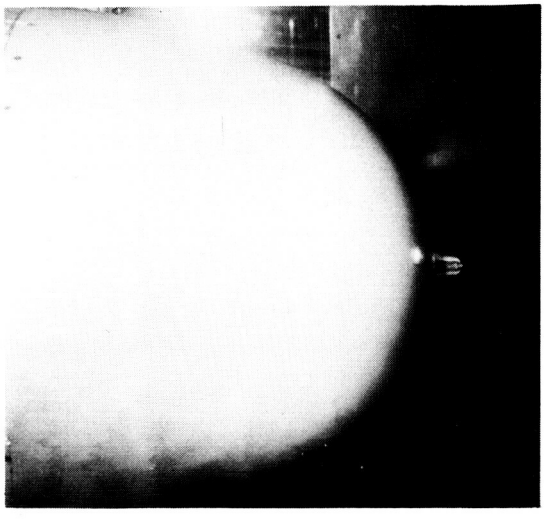

(a) Air temperature, 10° F. Front lighting.

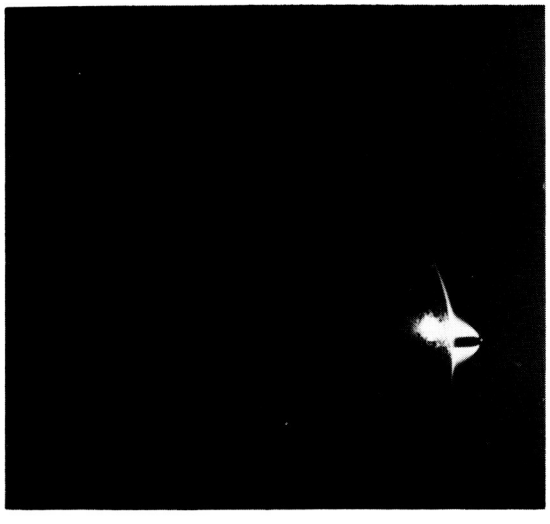

(b) Air temperature, 10° F. Back lighting.

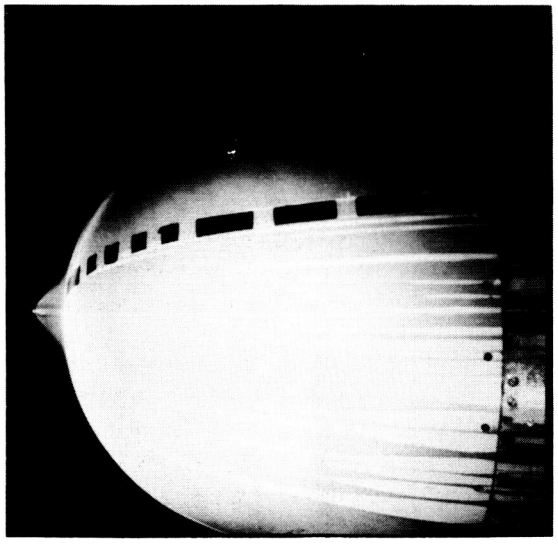

(c) Air temperature, -5° F.

Figure 23. - Views of glycol-water spray cone. T364M nozzle; nozzle air pressure, 46 pounds per square inch; velocity, 280 miles per hour; angle of attack, 0°; liquid-water content, 0 gram per cubic meter.

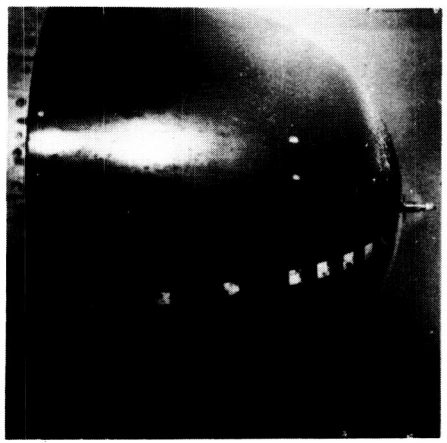

(a) Submarginal. Flow rate, 7.7 pounds per hour.

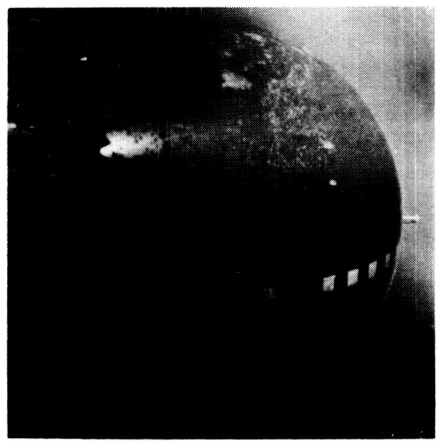

(b) Submarginal. Flow rate, 11 pounds per hour.

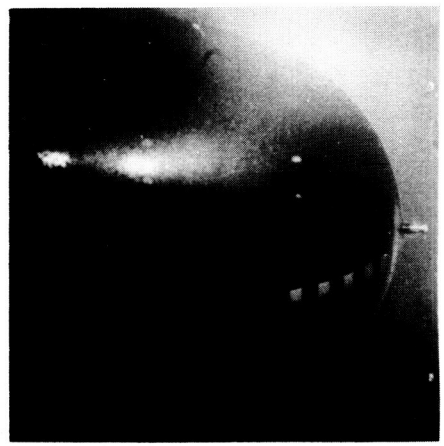

(c) Marginal. Flow rate, 12.5 pounds per hour.

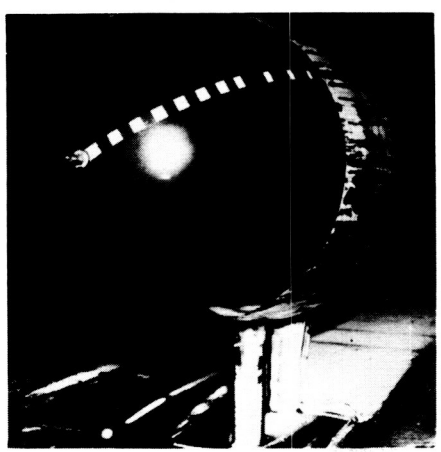

(d) Front view of model after shutdown.

(e) Rear view of model after shutdown.

Figure 24. - Views of D-radome during and after icing with glycol-water spray in use. Velocity, 267 miles per hour; angle of attack, 0°; tunnel total temperature, -15° F; liquid-water content, 0.75 gram per cubic meter.

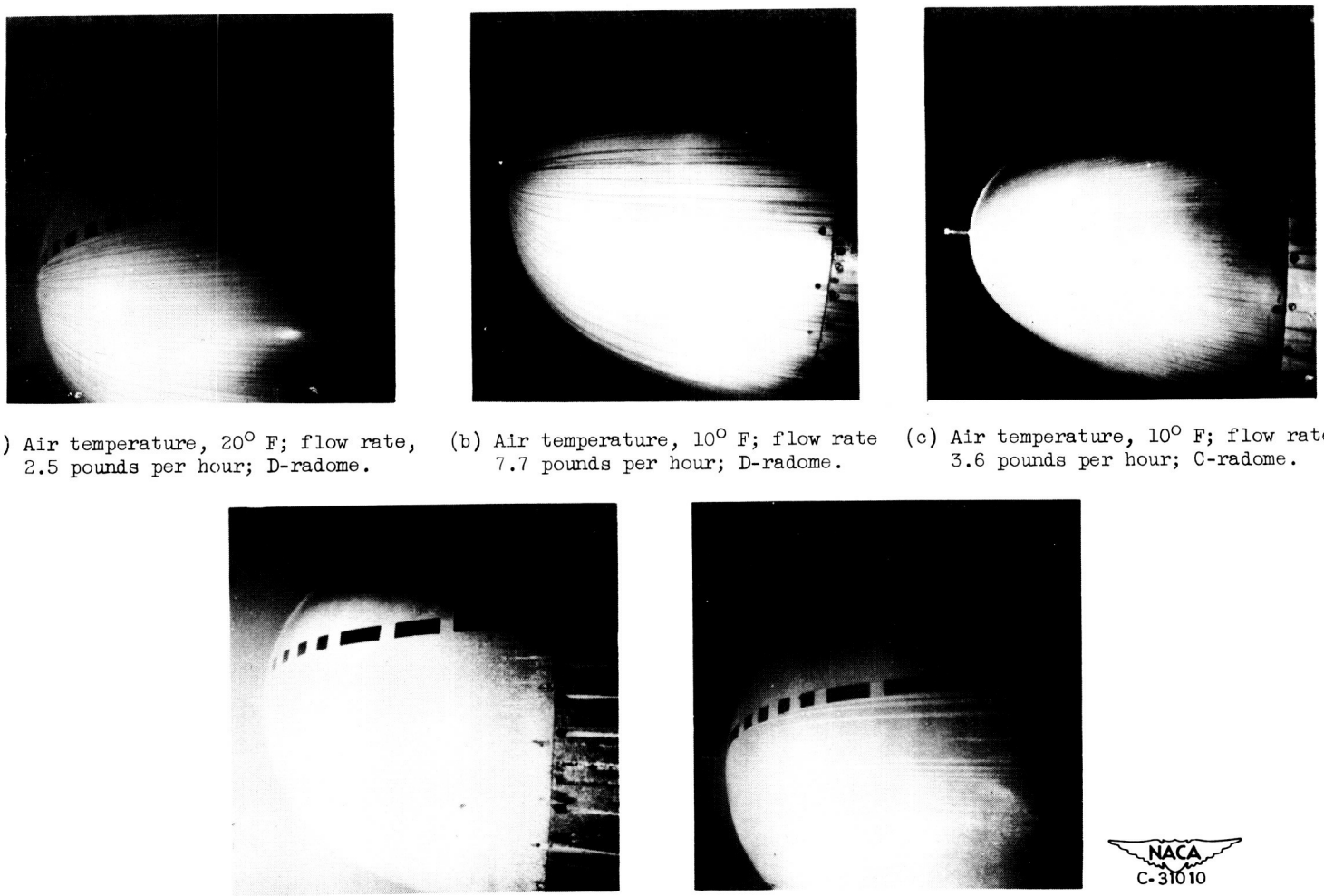

(a) Air temperature, 20° F; flow rate, 2.5 pounds per hour; D-radome.

(b) Air temperature, 10° F; flow rate 7.7 pounds per hour; D-radome.

(c) Air temperature, 10° F; flow rate, 3.6 pounds per hour; C-radome.

(d) Air temperature, -5° F; flow rate, 9.6 pounds per hour; D-radome.

(e) Air temperature, -13° F; flow rate, 14.5 pounds per hour; D-radome.

Figure 25. - Views of glycol-water flow on radome surface for marginal anti-icing condition and various tunnel total air temperatures. Velocity, 275 miles per hour; angle of attack, 0°; liquid-water content, 0.85 gram per cubic meter.

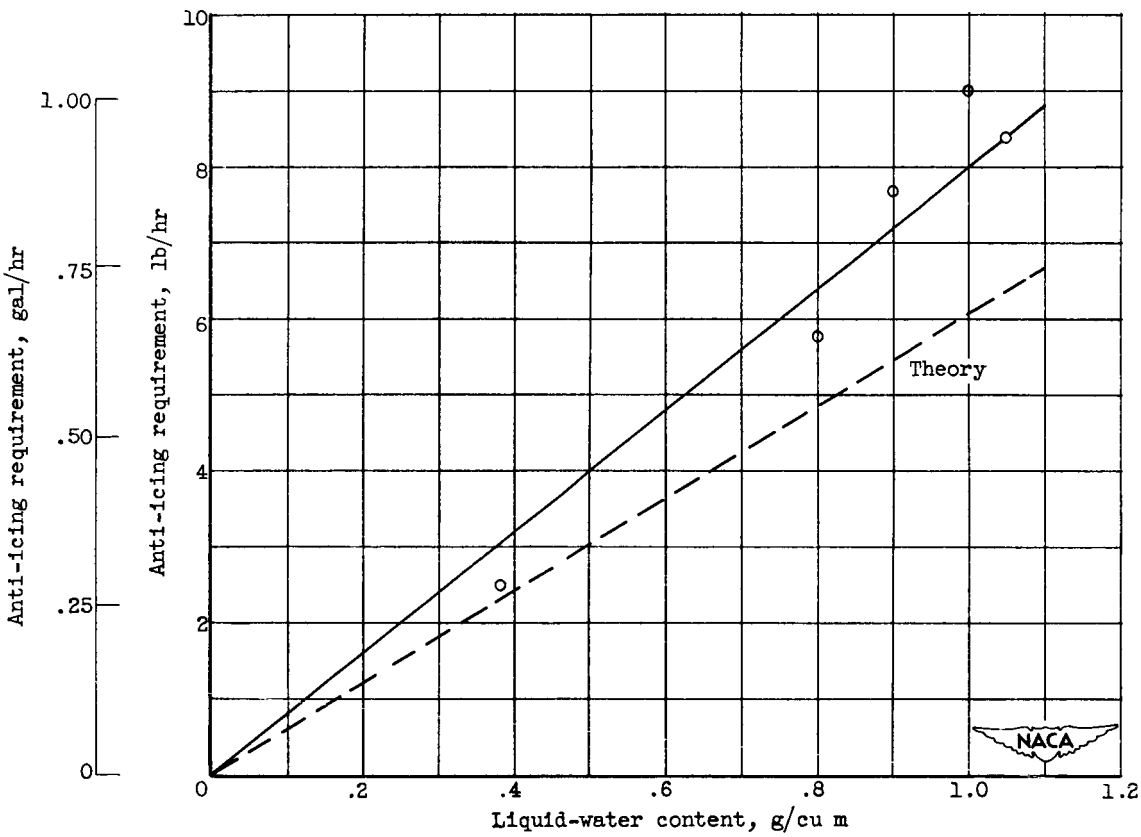

Figure 26. - Variation of fluid anti-icing requirement with liquid-water content. Velocity, 275 miles per hour; air total temperature, 10° F; angle of attack, 0°; F-89 D-radome; T364M nozzle.

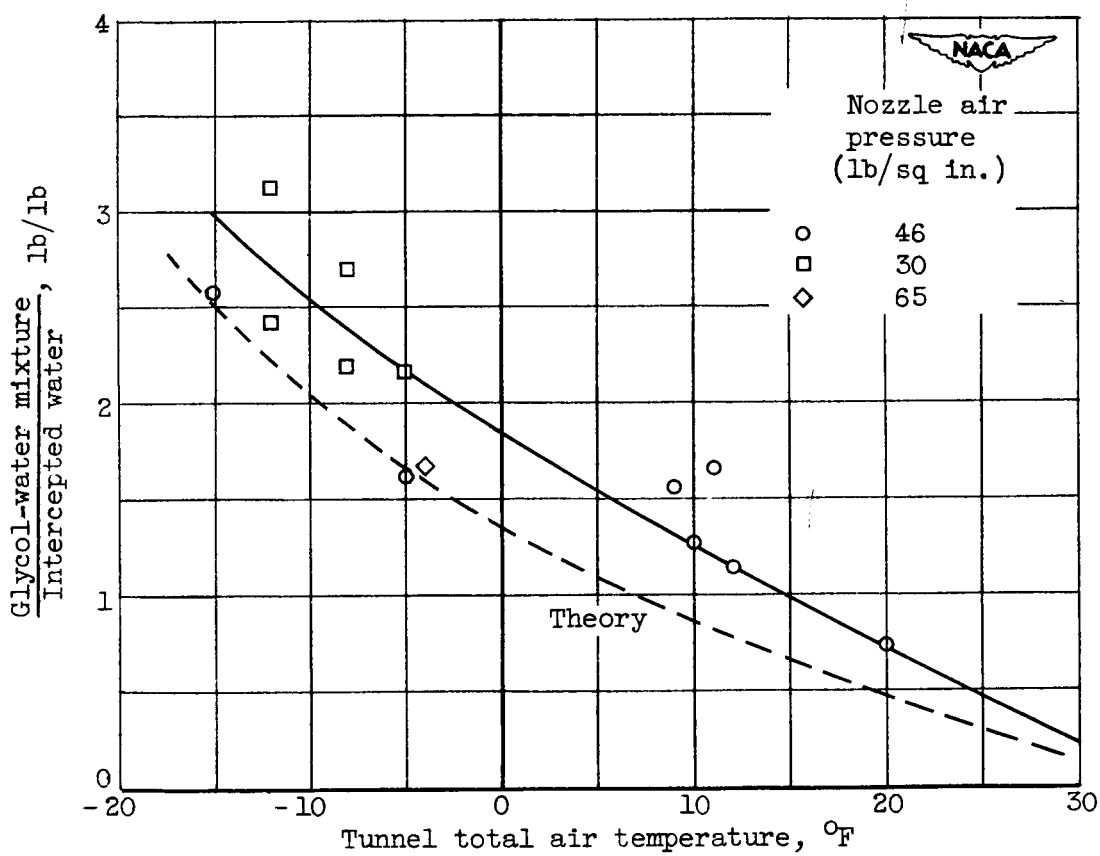

Figure 27. - Variation of fluid anti-icing requirement with air temperature. Velocity, 275 miles per hour; angle of attack, 0°; F-89 D-radome; T364M nozzle.

[redacted]

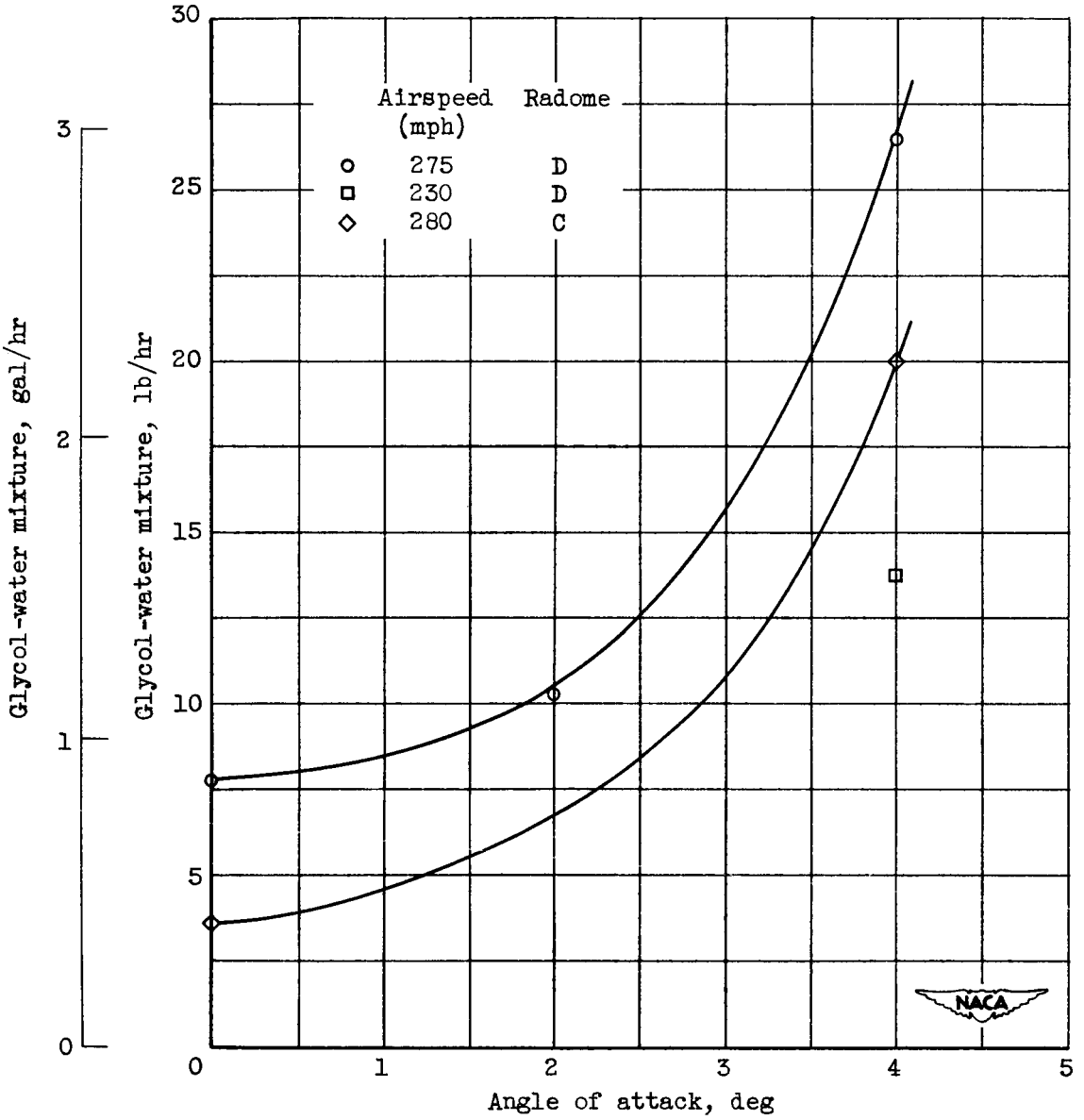

Figure 28. - Variation of fluid anti-icing requirement with angle of attack. Tunnel air temperature, 10° F; liquid-water content, 0.9 gram per cubic meter; T364M nozzle.

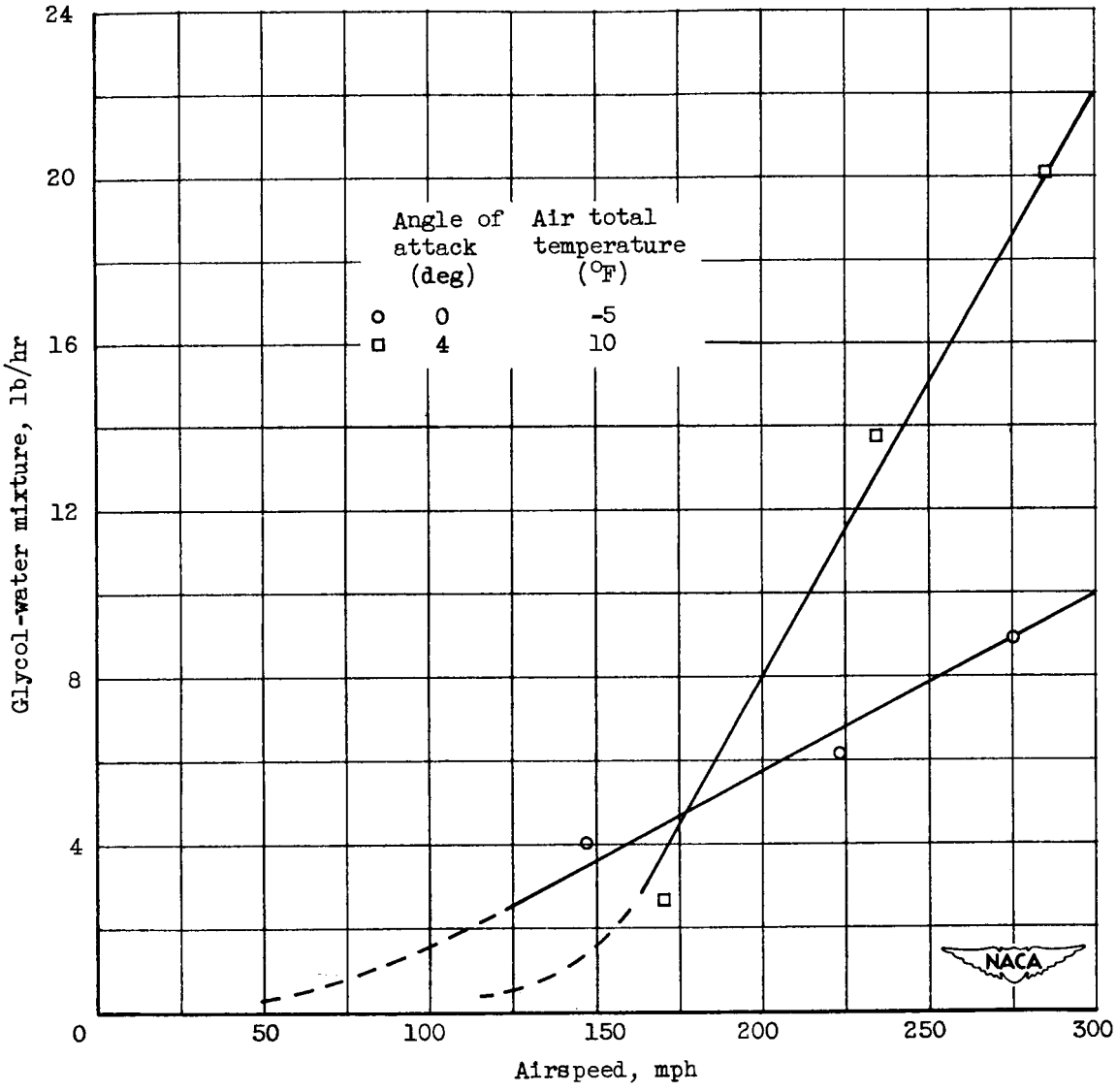

Figure 29. - Variation of fluid anti-icing requirement with airspeed for two angles of attack and two air total temperatures. Liquid-water content, 0.8 gram per cubic meter; D-radome; T364M nozzle.

[redacted]

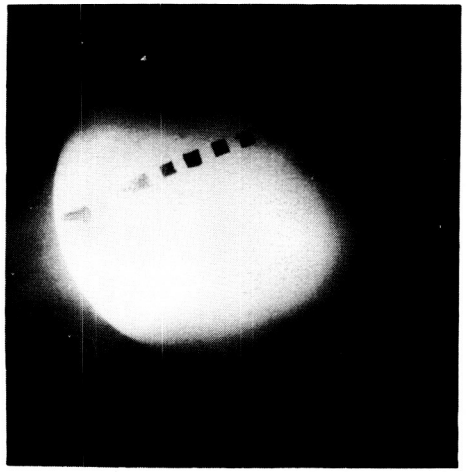

(a) After 5 minutes icing.

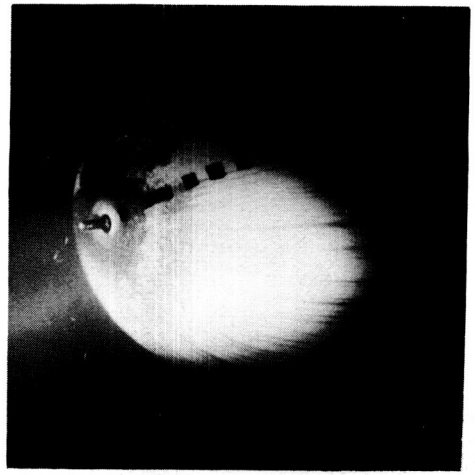

(b) 1 minute after glycol on.

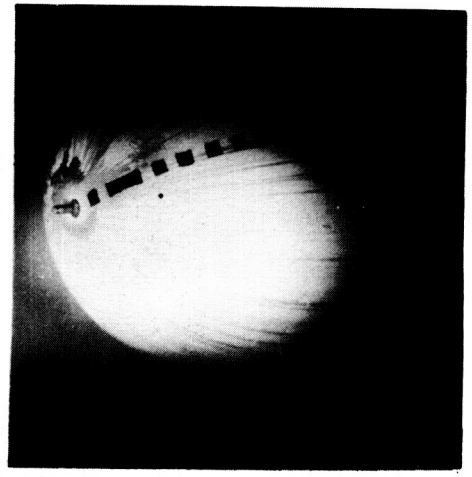

(c) 2 minutes after glycol on.

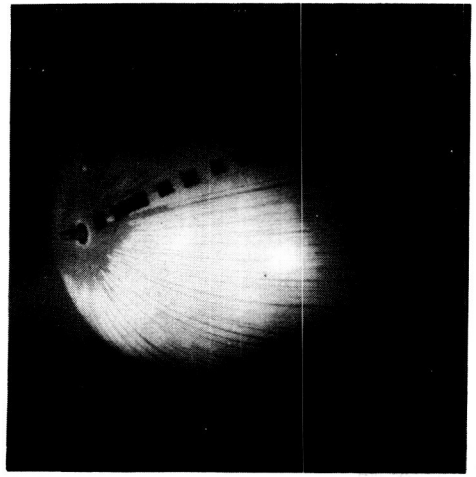

(d) 4 minutes 30 seconds after glycol on.

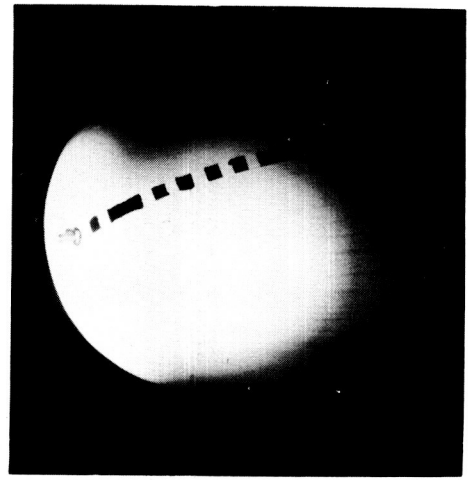

NACA
C-31011

(e) Cloud and glycol off.

Figure 30. - De-icing of D-radome. Velocity, 274 miles per hour; angle of attack, 0°; tunnel total temperature, 9° F; liquid-water content, 0.9 gram per cubic meter; glycol-water flow rate, 8.6 pounds per hour; T364M nozzle.

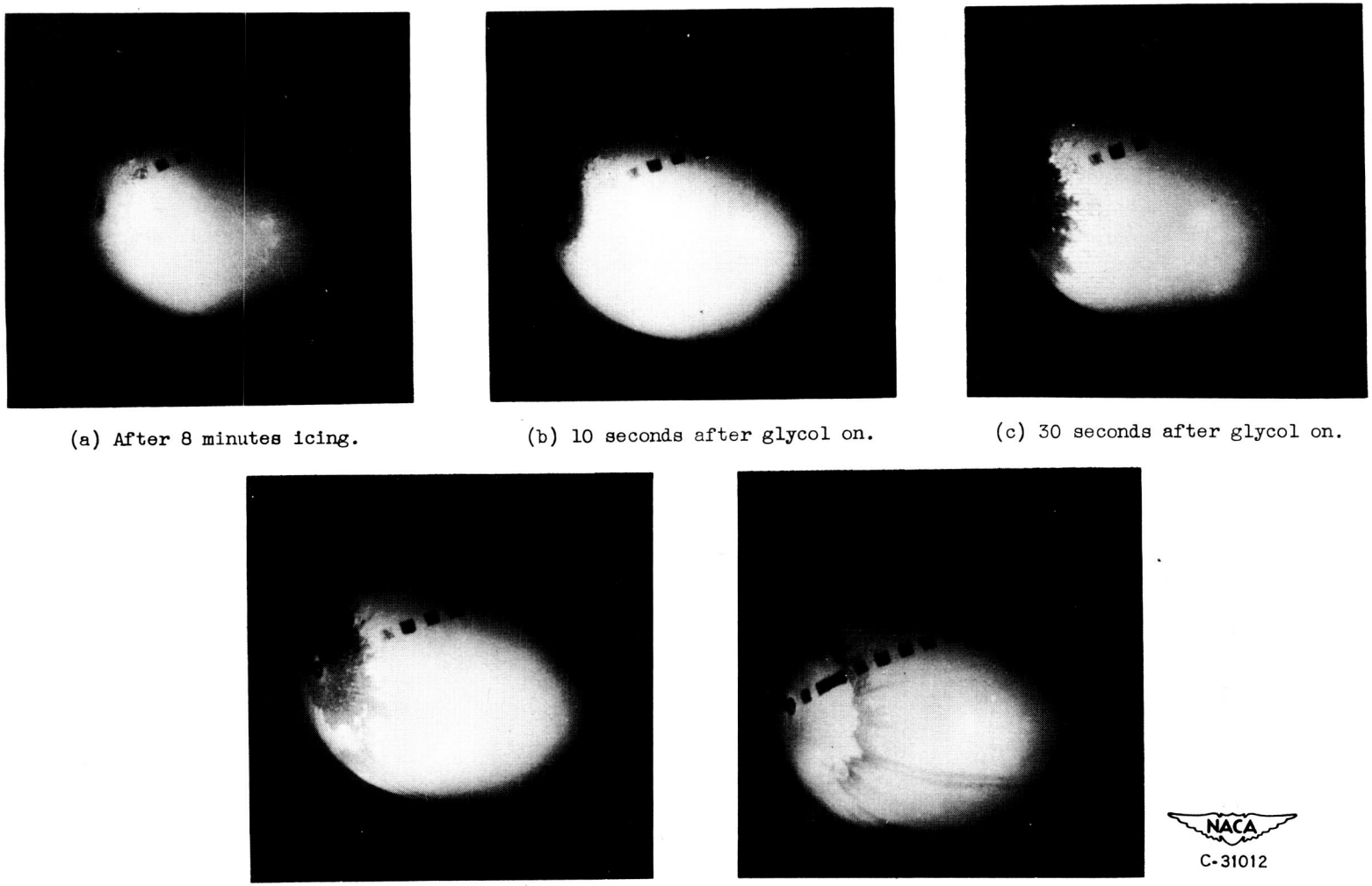

(a) After 8 minutes icing.

(b) 10 seconds after glycol on.

(c) 30 seconds after glycol on.

(d) 1 minute after glycol on.

(e) 2 minutes after glycol on.

Figure 31. - De-icing of D-radome. Velocity, 288 miles per hour; angle of attack, 2°; tunnel total temperature, 10° F; liquid-water content, 1.0 gram per cubic meter; glycol-water flow rate, 9 pounds per hour; T364M nozzle.

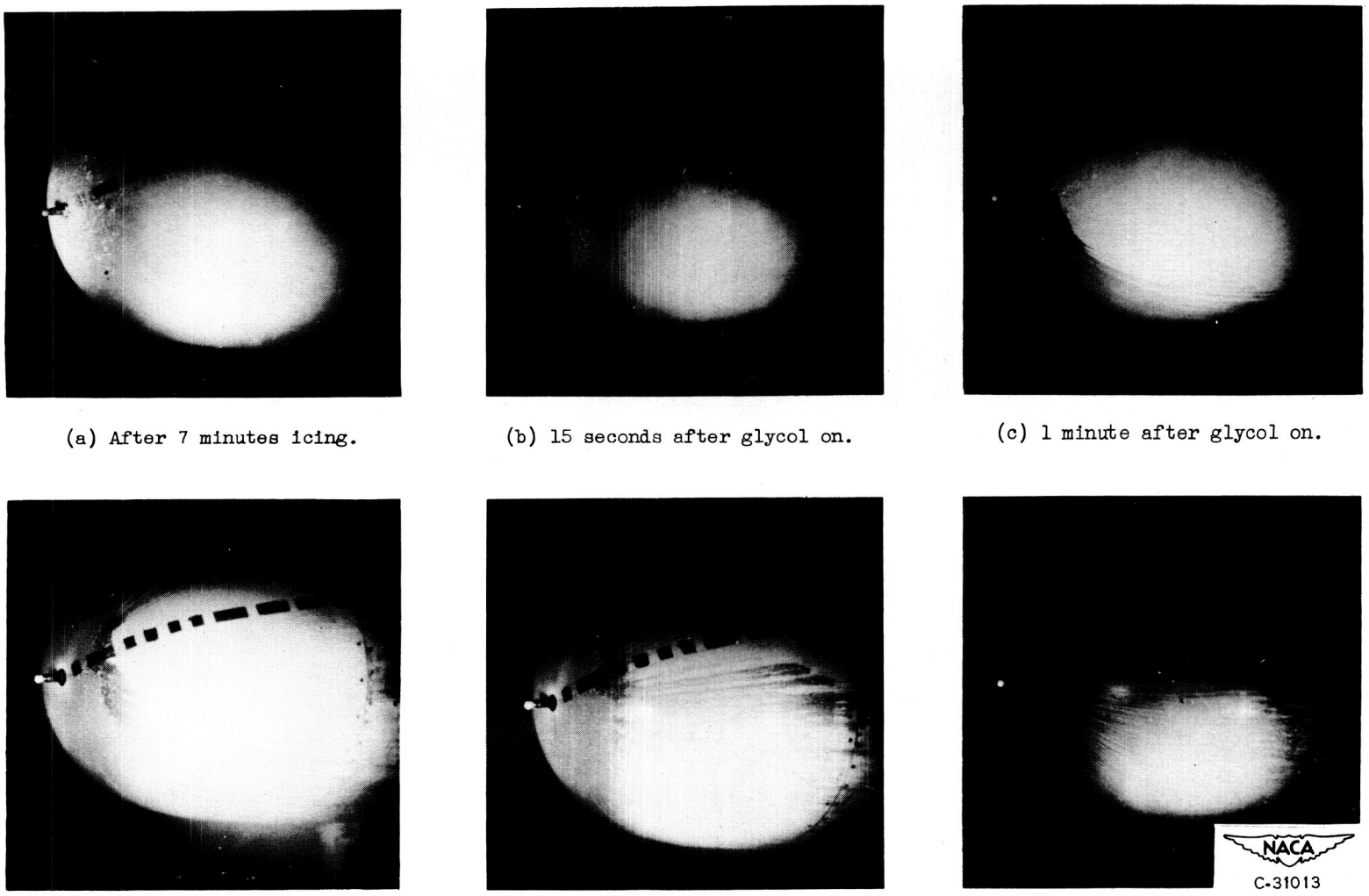

(a) After 7 minutes icing.

(b) 15 seconds after glycol on.

(c) 1 minute after glycol on.

(d) 2 minutes after glycol on.

(e) 3 minutes after glycol on.

(f) 5 minutes after glycol on.

Figure 32. - De-icing of D-radome. Velocity, 171 miles per hour; angle of attack, 4°; tunnel total temperature, 9° F; liquid-water content, 0.8 gram per cubic meter; glycol-water flow rate, 7.7 pounds per hour; T364M nozzle.

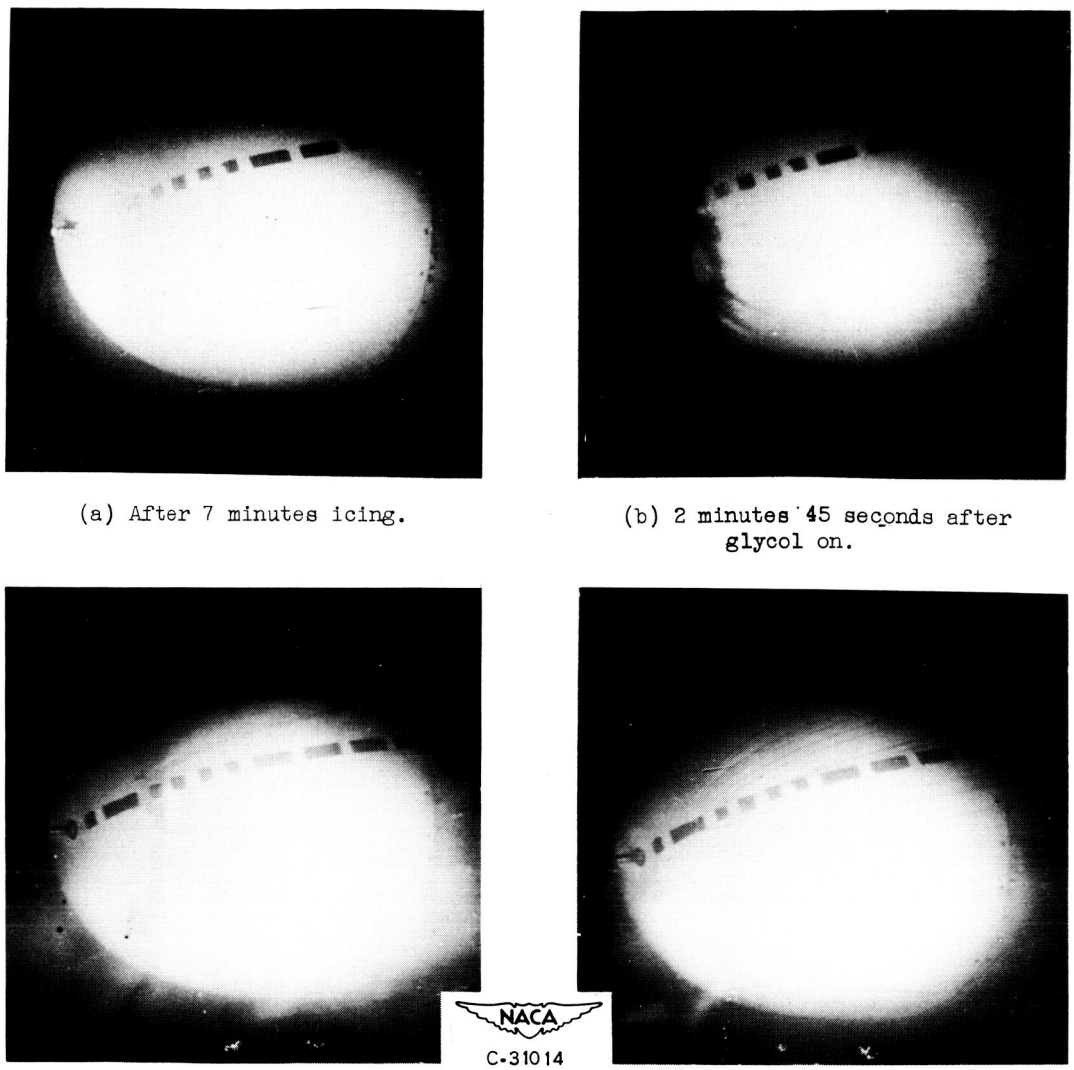

(a) After 7 minutes icing.

(b) 2 minutes 45 seconds after glycol on.

(c) 3 minutes after glycol on.

(d) 5 minutes after glycol on.

Figure 33. - De-icing of D-radome. Velocity, 283 miles per hour; angle of attack, 4°; tunnel total temperature, 9° F; liquid-water content, 1.0 gram per cubic meter; glycol-water flow rate, 31.8 pounds per hour; T364M nozzle.